Article

Structure-Based Prediction of Drug Distribution Across the Headgroup and Core Strata of a Phospholipid Bilayer Using Surrogate Phases

Senthil Natesan,[†] Viera Lukacova,[‡,∥] Ming Peng,[‡] Rajesh Subramaniam,[†] Sandra Lynch,[†] Zhanbin Wang,[†] Roman Tandlich,[§] and Stefan Balaz*,[†]

[†]Department of Pharmaceutical Sciences, Albany College of Pharmacy and Health Sciences, Vermont Campus, Colchester, Vermont 05446, United States

[‡]Department of Pharmaceutical Sciences, North Dakota State University, Fargo, North Dakota 58102, United States

[§]Division of Pharmaceutical Chemistry, Faculty of Pharmacy, Rhodes University, Grahamstown 6139, South Africa

Ⓢ Supporting Information

ABSTRACT: Solvation of drugs in the core (C) and headgroup (H) strata of phospholipid bilayers affects their physiological transport rates and accumulation. These characteristics, especially a complete drug distribution profile across the bilayer strata, are tedious to obtain experimentally, to the point that even simplified preferred locations are only available for a few dozen compounds. Recently, we showed that the partition coefficient (P) values in the system of hydrated diacetyl phosphatidylcholine (DAcPC) and n-hexadecane (C16), as surrogates of the H- and C-strata of the bilayer composed of the most abundant mammalian phospholipid, PC, agree well with the preferred bilayer location of compounds. High P values are typical for lipophiles accumulating in the core, and low P values are characteristic of cephalophiles preferring the headgroups. This simple pattern does not hold for most compounds, which usually have more even distribution and may also accumulate at the H/C interface. To model complete distribution, the correlates of solvation energies are needed for each drug state in the bilayer: (1) for the H-stratum it is the DAcPC/W P value, calculated as the ratio of the C16/W and C16/DAcPC (W for water) P values; (2) for the C-stratum, the C16/W P value; (3) for the H/C interface, the P values for all plausible molecular poses are characterized using the fragment DAcPC/W and C16/W solvation parameters for the parts of the molecule embedded in the H- and C-strata, respectively. The correlates, each scaled by two Collander coefficients, were used in a nonlinear, mass-balance based model of intrabilayer distribution, which was applied to the easily measurable overall P values of compounds in the DMPC (M = myristoyl) bilayers and monolayers as the dependent variables. The calibrated model for 107 neutral compounds explains 94% of experimental variance, achieves similar cross-validation levels, and agrees well with the nontrivial, experimentally determined bilayer locations for 27 compounds. The resulting structure-based prediction system for intrabilayer distribution will facilitate more realistic modeling of passive transport and drug interactions with those integral membrane proteins, which have the binding sites located in the bilayer, such as some enzymes, influx and efflux transporters, and receptors. If only overall bilayer accumulation is of interest, the 1-octanol/W P values suffice to model the studied set.

KEYWORDS: phospholipid, bilayer, phosphatidylcholine, DAcPC, DMPC, intrabilayer distribution, partition coefficient, headgroups, core, interface, n-hexadecane
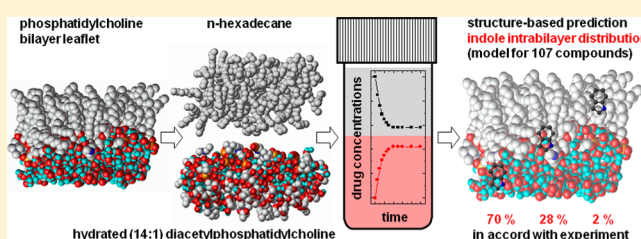
■ INTRODUCTION

The interactions with the headgroup (H) and core (C) strata of phospholipid bilayers play key roles in membrane protein folding[1] and channel function,[2] as well as in absorption and distribution of peptides, nucleic acids, drugs, and other small organic molecules in organisms.[3]

The bilayer H- and C-strata differ in the ability to shield electrostatic charges and in the types of interactions, in which the dissolved molecules participate. Despite intense thermal motion,[4] the strata are clearly distinguishable in neutron[5] and small-angle X-ray[6] diffraction experiments, as well as in molecular dynamics simulations[7] of the phosphatidylcholine (PC) bilayer. The main H- and C-strata can be further subdivided based on density,[7] voids,[8] and the average positions of PC fragments.[9] While most studies refer to individual layers as regions, we prefer to use the term "strata" so that the term "regions" can be reserved for distinct lateral areas (also called

lipid rafts) caused by immiscibility of some lipids in bilayer[10] or interactions of lipids with proteins,[11] cholesterol,[12] and other compounds.[13]

Among almost 200 known human lipid species, PC represents 42−49% of phospholipids and 0.7−2.5% w/w of fresh tissue (containing 70−80% of water), for skeletal muscle,[14,15] heart, and liver.[15] Linoleic acid (18:2) with 37.7% is the most abundant fatty acid in PC of human skeletal muscle, followed by palmitic acid (16:0) with 27.3% and oleic acid (18:1) with 14.0%.[16] In the adipose tissue, the contents are 10%, 23%, and 48%, respectively.[15] Considering a usual pattern, a saturated acid and an unsaturated acid esterifying the PC glycerol's O-1 and O-2 atoms, respectively, it can be inferred that 1-palmitoyl-2-linoleoyl-sn-glycero-3-phosphocholine and 1-palmitoyl-2-oleoyl-sn-glycero-3-phosphocholine are the most abundant phospholipid molecules in skeletal muscle and adipose tissue, respectively. While the lipid diversity plays significant roles in physiological processes, most partition data have been obtained with PC containing saturated fatty acids because of easier synthesis and resistance to oxidation. Among them, dimyristoylphosphatidylcholine (DMPC) was used most frequently thanks to a lower transition temperature, oxidation stability, and availability, although a recent study pointed out that DMPC and other PC bilayers may differ in accumulation of some compounds.[17]

Several complementary experimental methods, mainly wide-angle[18,19] (WAXS) and small-angle X-ray scattering (SAXS)[20,21] and neutron diffraction,[17,22−24] various nuclear magnetic resonance (NMR)[25−28] and electron paramagnetic resonance (EPR)[29] techniques, surface plasmon resonance,[30] as well as fluorescence[31] and fluorescence quenching,[32] have been used for characterization of the preferred location of compounds in the phospholipid bilayer.[33] Except WAXS, SAXS, and neutron diffraction, these methods usually do not provide a complete intrabilayer distribution profile. All methods are tedious and not amenable to a higher throughput. On a routine scale, typically only the overall bilayer partitioning is measured, without obtaining the details pertinent to individual bilayer strata.

To extrapolate the valuable bilayer location data to other compounds and quickly obtain estimates of solvation free energies of chemicals in the bilayers or their strata, organic solvents have been examined as surrogates. The partition coefficients P in two solvent systems, which are *capable of similar interactions* with the studied compounds, are related according to the Collander equation:[34]

$$P_2 = \alpha P_1^\beta \tag{1}$$

The parameters α and β are obtained by the fit to experimental data. The approach is widely used in the design of bioactive compounds,[35] computational chemistry,[36] protein folding,[37] and other areas.[38] The Collander equation (eq 1) is one of the numerous extrathermodynamic relationships, which include linear free energy relationships (LFERs),[39] and cover a broad area of physical organic chemistry. The LFERs describe correlations between free or activation energy changes with chemical structure, in two or more processes. Such changes in reference processes can be used to define LFER parameters characterizing individual substructures, such as the Hammett constants[40] and fragment solvation characteristics,[35] or entire molecules such as solvatochromic parameters.[39,41] The requirement of similarity of the two processes holds for simple linear correlations, such as the logarithmized Collander equation (eq 1), but may be waived if multiple LFER parameters are used.

Additive-constitutive nature of the partition coefficient P provides for its deconvolution into the solvation characteristics (f) of structural fragments. This trait allows prediction of the P values from structure and the modeling of partitioning of amphiphilic molecules, which may interact with the H/C interface and protrude in both H- and C-strata. The f values in the surrogate phases for individual strata can be summed up to estimate the overall solvation free energy. The f values represent enthalpy and entropy changes upon transfer of individual fragments between the strata. The additional entropy changes associated with the entire molecule are not treated explicitly but are, to some extent, accommodated by the enthalpy−entropy compensation, which is a common phenomenon in partitioning.[42−44] The two attributes of the P values, Collander scaling (eq 1) and additive-constitutive nature, create the basis for the development of the reference systems, such as the widely used 1-octanol/water (O/W) system, and also lie at the heart of the present approach.

The key issue for the selection of a proper surrogate is the similarity of interactions with the imitated system. In this aspect, diacetyl phosphatidylcholine (DAcPC) contains all structural fragments and represents the closest match to the PC headgroup. High aqueous solubility of DAcPC allows its use in the hydration state close to that of a fluid PC bilayer at room and body temperatures, represented by 6−16 water molecules per a headgroup,[45−48] and making hydrated DAcPC a potential surrogate phase of the H-stratum of the PC bilayer. Whether the lacking anisotropy and the racemic nature of hydrated DAcPC affect its ability to emulate solvation behavior of a PC bilayer remains to be seen.

Hydrocarbons are appropriate core surrogates as evidenced by experimental observation of similar molecular packing[49] and dynamics[50] of the fatty acyl chains in the core of the bilayer and in bulk liquid alkanes. The studies with black lipid membranes show that the selectivity of the bilayer in the partitioning of the H-bonding groups lies somewhere between those of 1-octanol and alkanes[51,52] or alkenes[53] but is significantly closer to the latter solvents for the studied compounds.

DAcPC, when dissolved in water in molar ratio 1:14 used in our experiments, forms a homogeneous, isotropic, and only slightly viscous solution.[54] The DAcPC molecules do not measurably partition from this solution into *n*-hexadecane (C16) in the two-phase system. We showed that the C16/DAcPC partition coefficients perfectly discriminate between the lipophiles accumulating in the core and cephalophiles preferring the H-stratum, in contrast to the O/W and C16/W partition coefficients alone or their ratio.[55] This observation indicates the suitability of hydrated DAcPC and C16 as the surrogate phases of the H- and C-strata.

As criteria for selecting a proper surrogate, early studies used partitioning into cells and transport through multicellular biological films, which are both affected by protein binding, multiplicity of bilayers, and other factors. These problems are avoided when using unilamellar phospholipid liposomes, which are more suitable for evaluation of the surrogate phases. Liposome partitioning depends on the temperature, which should be well above the gel−fluid phase transition temperature,[56] fluidity,[57] phospholipid surface density,[58] and other related factors.[59]

Computational approaches for studying macromolecules and drugs in the bilayer have used different levels of approximation

for the bilayer structure, ranging from implicit continuum models, to coarse-grained mesoscale models,[60] to fully atomistic representations.[61] Our approach formally represents a simple model belonging to the first category.

Continuum approaches started with conformational optimization using a classical force field in a pure hydrocarbon slab immersed in water, with different dielectric constants for the aqueous and nonpolar phases.[62] Initial insertion of chemicals and peptides was guided by the hydrophobic and hydrophilic centers of the molecules, which were determined using the atomic O/W transfer energies.[63] A hydrophobic potential energy function was devised to represent the bilayer environment[64] and combined with a cavity formation term.[65] The depth-dependent dielectric constant and atomic hydrophobicity parameters were used to estimate the solute solvation energies in the bilayer.[66] A restrain function was developed to generate peptide conformations typical for bilayers.[67] All these studies relied on the O/W and alkane/W partitioning data, which, as we have shown,[55] do not correctly emulate solvation in bilayer strata as they fail to identify the cephalophiles and lipophiles accumulating in the H- and C-strata of the PC bilayer. Solvation energies can be estimated using two components: (1) intramolecular electrostatic energy, calculated by classical or quantum mechanical techniques and (2) the "nonpolar" energy spent for cavity formation and released by interactions with the solvent, approximated by techniques based on the atomic solvent-accessible surface area (SASA) combined with empirical atomic surface tensions, derived from partition experiments.[68] A well-known application to different solvents is represented by the series of the SMx models.[69] The two-component concept was applied to bilayer solvation in several studies differing in sophistication of the model setup and used computational techniques. A simple hexane slab was used to study the preferred bilayer location of steroids,[70] with the finite-difference solutions to the Poisson equation providing the electrostatic part,[71] and a linear relation to the SASA defining the nonpolar part. A multistrata dielectric model setup was used to study membrane proteins in combination with generalized Born electrostatics and the SASA multiplied by a depth-dependent function, which was obtained from the free-energy profile of oxygen in the bilayer, generated by molecular dynamics (MD) simulation.[72] Similar techniques have been implemented in the CHARMM package.[73] A multistrata, continuum COSMOmic (mic for micelle) approach[74] is built around the density functional theory (DFT) calculations combined with conductor-like screening model for realistic solvation (COSMO-RS).[75] The bilayer details are obtained from atomistic MD simulations, allowing for study of mixed bilayers.[76,77] A detailed PPM (Positioning of Proteins in Membranes) approach combines the trans-bilayer profiles of the dielectric constant and some solvatochromic parameters[39,41] with the electrostatics calculated using the dipole moments rather than atomic charges for nonpolar solutes and the Born equation for ions.[78,79]

Mesoscale models were mainly used in the MD studies of structural aspects of bilayer dynamics and were deemed unsuitable for partitioning of small molecules.[80] This situation is gradually changing with the development of more sophisticated coarse-grained force fields, which can be smoothly transformed to atomistic models in the areas of interest.[81−83]

Atomistic MD simulations were used to analyze bilayer interactions with small molecules, with the first studies focusing on benzene,[84,85] dimethyl 1,4-dihydro-2,6-dimethyl-4-(2-methylphenyl)-3,5-pyridinedicarboxylate (a nifedipine analogue),[86] trichloroethylene,[87] and a 29 amino acid fragment of corticotropin-releasing factor.[88] Numerous other MD studies revealed several important aspects of trans-bilayer diffusion, such as varying diffusion rates in individual strata, a faster speed of lateral than transversal diffusion,[84] and a preferred longitudinal orientation of transported molecules along the bilayer normal in the most dense interfacial stratum, unless strong H-bonds are formed.[89] Several studies emphasized preferred molecular positions and orientations during the diffusion process.[90,91] Free-energy estimates were obtained using various biasing MD techniques, to reduce the computing time.[92] These data are getting more precise with the development of specialized force fields for lipids.[93−95] The force fields were compared for their ability to reproduce the bilayer characteristics and the overall bilayer/water partition coefficients of several compounds.[96]

Here we present a simple continuum approach that uses a coarser representation of the PC bilayer than the most detailed continuum models: the homogeneous H- and C-strata, connected through a planar H/C-interface passing right below the fatty acid ester groups of PC. This simplification allows us to directly use the solvation energies of molecules and their fragments, which were obtained from partitioning experiments with relevant surrogate phases. We hypothesize that quantitative estimates of the intrabilayer drug distribution can be obtained by modeling measured overall partitioning of compounds into the DMPC bilayers in unilamellar liposomes and the DMPC monolayers adsorbed on nonporous, octadecylated silica microparticles. All reasonable interfacial poses of each molecule are examined in the model. To reduce complexity in generating the poses, simple molecules with reduced conformational flexibility and avoiding ionization under physiological conditions were selected. The correlation also provides, for each compound, estimated distribution in bilayer strata, including the preferred pose(s) at the H/C interface. The predictions of preferred location in the PC bilayer are compared with experimental data for the compounds, where this information exists.

■ EXPERIMENTAL SECTION

Chemicals. DAcPC was obtained from Euticals (Prime European Therapeuticals S.p.A, Lodi, Italy). All studied solutes (Table 1) and C16 were purchased from Sigma-Aldrich (St. Louis, MO).

C16/DAcPC and C16/W Partitioning. The experiments in the pre-equilibrated, stirred two-phase systems were described in detail previously.[55,97] The kinetics of partitioning was monitored, in both phases when feasible, to make sure that the equilibrium concentrations were determined. The compounds were analyzed by UV−Vis, HPLC, or GC/MS after SPME extraction as appropriate. Evaporation was accounted for and the compounds were checked for instability and self-aggregation under experimental conditions.

Partitioning to Phospholipid Monolayers. Preparation of DMPC monoloayers on octadecylated, nonporous silica particles of uniform size was described previously, along with the partition experiments.[98]

Partitioning to Liposomes. *Liposome Preparation.* Unilamellar DMPC liposomes with diameters of about 80 nm were prepared by the extrusion method[99] using a mini-extruder (Avanti Polar Lipids, Alabaster, AL) with 0.1 μm filter (Nucleopore polycarbonate Track-Etch membrane, Whatman, Florham Park, NJ) at 37 °C. Before extrusion, powdered

Table 1. Studied Compounds, Partition Coefficients (*P*) in the Solvent and PC Systems, Number of Possible Interfacial Poses (NP), and Predicted Fractions in Bilayer Strata

| | | | | | logP | | | | | relative amount (%)[h] | | |
| | | | | | monolayer/W | | bilayer/W | | | | | |
no.	compound name	C16/W[a]	C16/DAcPC[b]	O/W[c]	exptl[d]	calcd[e]	exptl[f]	calcd[e]	NP[g]	H	I	C
1	1,2-dichlorobenzene	3.52[i]	2.24	3.43	3.28[o]	3.28	3.33	3.28	13	10	20	70
2	1,3,5-trichlorobenzene	4.48[i]	2.89	4.19	3.71[o]	4.15	3.95[q]	4.12	10	2	17	81
3	1,3-dichlorobenzene	3.69[i]	2.46	3.53	3.22[o]	3.50	3.03	3.51	15	5	35	60
4	1,3-dimethyl-2-nitrobenzene	2.48	1.80	2.95	2.52	2.69	2.99	2.78	12	22	55	23
5	1,4-dichlorobenzene	3.70[i]	2.41	3.44	3.22[o]	3.43	3.56	3.40	7	7	16	77
6	1,4-dimethylbenzene	3.25	2.59	3.15	3.49[o]	3.00	2.98[q]	2.98	7	14	9	77
7	1-bromo-2-phenylethane	2.35[i]	2.07	3.09	2.89	2.81	2.71	2.93	16	13	75	12
8	1-bromo-3-phenylpropane	3.66	2.18	3.72	3.95	3.60	3.04	3.65	18	4	55	40
9	1-bromo-4-chlorobenzene	3.78	3.34	3.54	3.24	3.50		3.47	14	4	17	79
10	1-bromonaphthalene	4.17	3.43	4.06	3.96	3.91		3.90	18	2	30	68
11	1-hexanol	0.44	−0.01[l]	2.03		2.55	1.91[q]	2.69	12	24	76	0
12	1-naphthaldehyde	2.21	1.36	2.67[n]	2.62[o]	2.41	2.80[o]	2.49	16	47	29	25
13	1-naphthol	0.44[i]	−1.18	2.85	2.82	2.43	2.80	2.58	17	56	43	0
14	2,2′,3,3′,4,4′-hexachlorobiphenyl	5.98	8.36	7.32		5.53	6.09[q]	5.47	9	0	5	95
15	2,2′,3,3′,4,5,5′,6-octachlorobiphenyl	7.25	10.37[l]	8.16[n]		6.71	6.18[q]	6.66	16	0	1	99
16	2,2′,3,3′,4-pentachlorobiphenyl	5.98	7.35	6.30	5.94	5.53		5.47	16	0	5	95
17	2,2′,3,3′,6,6′-hexachlorobiphenyl	5.98	8.36	7.12		5.53	5.90[q]	5.47	8	0	5	95
18	2,2′,3,3′-tetrachlorobiphenyl	5.35	6.35	6.18	-	4.93	5.40[q]	4.88	8	0	5	95
19	2,2′,3,4,4′,5,5′-heptachlorobiphenyl	7.25	8.90	8.16[n]	6.91[p]	6.72	6.33[q]	6.66	16	0	2	98
20	2,2′,3,5,6′-pentachlorobiphenyl	6.14	6.89	6.72[n]	6.21	5.72		5.69	16	0	19	81
21	2,2′,3,5′-tetrachlorobiphenyl	5.83	5.88	5.81	5.47[o]	5.38		5.33	8	0	5	95
22	2,2′,3,6-tetrachlorobiphenyl	5.35	6.35	6.01[n]	4.99[o]	4.99		4.96	15	0	22	78
23	2,2′,3-trichlorobiphenyl	5.04	5.34	5.60	5.26[o]	4.68		4.66	14	0	20	80
24	2,2′,4,4′,6,6′-hexachlorobiphenyl	6.49[j]	7.43	7.29		6.06	6.00[p]	6.04	9	0	22	78
25	2,2′,4,5,5′-pentachlorobiphenyl	6.62	6.42	6.85	5.68[o]	6.14		6.10	16	0	10	90
26	2,2′,4,5-tetrachlorobiphenyl	5.83	5.88	6.27	5.96[p]	5.43	5.55[q]	5.40	16	0	20	80
27	2,2′,4,5′-tetrachlorobiphenyl	6.30	5.42	6.36	6.26	5.84		5.80	9	0	9	91
28	2,2′,4-trichlorobiphenyl	5.51	4.88	5.76	5.06[o]	5.15	5.03	5.14	16	0	25	74
29	2,2′,5,5′-tetrachlorobiphenyl	6.27[j]	5.42	6.26	5.69[o]	5.80		5.75	8	0	6	94
30	2,2′,5-trichlorobiphenyl	5.51	4.88	5.60	4.92[p]	5.14		5.12	15	0	22	78
31	2,2′,6-trichlorobiphenyl	5.04	5.34	5.47	4.70[o]	4.68		4.65	8	0	19	81
32	2,2-diphenylethanol	1.05[i]	−0.08	2.77[n]	2.99	2.32	2.34	2.46	8	58	40	2
33	2,2′-dichlorobiphenyl	4.72	4.33	4.97	4.37[o]	4.38		4.35	7	1	19	81
34	2,3,3′,6-tetrachlorobiphenyl	5.83	5.88	6.26[n]	5.47[o]	5.38		5.33	13	0	6	94
35	2,3,4,5,6-pentachlorobiphenyl	6.62	7.82[l]	6.74		6.12	5.90[q]	6.06	16	0	1	99
36	2,3,4,5-tetrachlorobiphenyl	5.83	6.35	6.41		5.39	5.44[q]	5.35	16	0	9	91
37	2,3,4′,6-tetrachlorobiphenyl	5.83	5.88	6.26[n]	6.07	5.40		5.35	13	0	10	90
38	2,3′,4-trichlorobiphenyl	5.99	4.41	5.92[n]	5.10[o]	5.55		5.50	10	0	10	90
39	2,3′,5-trichlorobiphenyl	5.99	4.41	5.76	4.74[o]	5.54		5.48	10	0	6	94
40	2,3,6-trichlorobiphenyl	5.04	5.34	5.67	5.00[o]	4.69		4.67	15	0	23	77
41	2,3′,6-trichlorobiphenyl	5.51	4.88	5.67	5.00[o]	5.14		5.12	15	0	23	77
42	2,3-diaminonaphthalene	−0.22	−1.70[m]	1.54	2.39	2.30		2.44	21	72	28	0
43	2,3-dichlorobiphenyl	4.72	4.33	4.99	4.85[o]	4.40		4.37	14	0	23	77
44	2,3′-dichlorobiphenyl	5.20	3.87	5.02	4.53[p]	4.84		4.82	10	0	22	77
45	2,4,5-trichloroaniline	2.14	1.04	3.69	3.31[o]	3.36	3.58[p]	3.50	19	5	93	2
46	2,4,5-trichlorobiphenyl	5.74[i]	4.88	5.90		5.33	5.16[q]	5.29	16	0	15	85
47	2,4,6-trichlorobiphenyl	5.51	4.88	5.71		5.15	4.71[q]	5.14	16	0	26	74
48	2,4′,6-trichlorobiphenyl	5.51	4.88	5.75	5.26[o]	5.15		5.14	16	0	26	74
49	2,4-dichlorobiphenyl	5.20	3.87	5.30	4.91[o]	4.86		4.84	16	0	26	74
50	2,4′-dichlorobiphenyl	5.20	3.87	5.10	4.85[o]	4.86		4.84	15	0	26	74
51	2,5-dichlorobiphenyl	5.20	3.87	5.16	4.91[o]	4.84		4.82	14	0	23	77
52	2,5-dimethylphenol	0.37[i]	0.36	2.33	2.32	2.03		2.17	13	65	34	1
53	2,6-dichlorobiphenyl	4.72	4.33	4.98	4.37[o]	4.38		4.36	11	1	20	80
54	2,6-dimethoxyphenol	−2.28	−1.14	1.15	1.99	1.64	1.65	1.78	9	89	11	0
55	2-bromonaphthalene	4.17	3.43	4.18[n]	4.05	3.92		3.92	20	2	32	66
56	2-bromostyrene	3.73	3.32	3.73[n]	3.20	3.49		3.48	12	4	27	69
57	2-bromotoluene	3.50	3.46	3.50	3.40	3.29		3.29	16	5	30	65

Table 1. continued

		logP			monolayer/W		bilayer/W			relative amount (%)[h]		
no.	compound name	C16/W[a]	C16/DAcPC[b]	O/W[c]	exptl[d]	calcd[e]	exptl[f]	calcd[e]	NP[g]	H	I	C
58	2-chlorobiphenyl	4.41	3.33	4.53	4.24[p]	4.09	4.09	4.07	7	1	20	79
59	2-hydroxybiphenyl	0.75	−0.15	3.09	3.15[o]	2.27	3.21[p]	2.42	15	57	42	1
60	2-methylanthracene	5.05	3.41	5.00	4.15	4.76		4.76	23	0	36	64
61	2-nitroaniline	0.22[i]	−0.89	1.85	1.99	2.49	2.45	2.64	15	38	62	0
62	2-nitrotoluene	2.25[i]	1.22	2.30	2.34	2.48	2.41[q]	2.57	15	43	34	23
63	3-bromoaniline	1.04[k]	−0.15	2.10	2.10	2.44	2.36	2.58	17	45	53	2
64	3-nitroaniline	−0.68[i]	−1.41	1.37	2.18[o]	2.02	2.17[q]	2.16	16	94	6	0
65	3-nitrotoluene	1.81	1.29	2.45	2.60	2.41	2.56	2.53	18	37	54	9
66	4,4′-dichlorobiphenyl	5.67	3.41	5.58		5.21	4.78[q]	5.25	9	0	11	89
67	4-amino-3-methylphenol	−2.63	−1.19[m]	0.70[n]	1.80[o]	1.53	1.41[p]	1.68	15	99	1	0
68	4-aminoacetophenone	−0.70[i]	−1.95	0.86	1.67	2.11		2.26	12	97	3	0
69	4-aminophenol	−3.34	−3.04	0.04	1.76	1.77	1.82	1.91	14	100	0	0
70	4-biphenylcarboxaldehyde	3.01	2.18	3.38[n]	3.08[o]	2.99	3.14[r]	3.04	23	13	47	40
71	4-bromoaniline	0.65	−0.26	2.11	2.92	2.31	2.47	2.45	14	53	46	1
72	4-bromobenzophenone	2.46[k]	2.43	4.12[n]	2.58	2.53	2.66	2.59	14	25	42	34
73	4-bromophenol	−0.01[i]	−1.20	2.59	2.56	2.40	3.01	2.55	14	48	51	0
74	4-chloro-3-methylphenol	0.22[k]	−1.08	3.10	2.73[o]	2.97	3.19[p]	3.12	16	14	86	0
75	4-chlorobenzophenone	2.86[k]	2.49	3.79	3.45	2.78	2.57[p]	2.81	14	18	33	49
76	4-chlorotoluene	3.48	2.47	3.33	3.06[o]	3.25		3.24	14	9	21	70
77	4-dimethylamino-benzaldehyde	2.50	0.05	2.01	1.83	2.62		2.69	14	65	6	29
78	4-nitroaniline	−0.72[k]	−2.23	1.39	2.16	2.17	2.01	2.32	14	96	4	0
79	4-nitrotoluene	1.81	1.20	2.37	2.10	2.37	2.40	2.49	14	42	47	10
80	4-n-pentylphenol	2.11	0.89[l]	4.24		4.17	4.31[q]	4.02	22	1	98	0
81	4-phenoxybutyl bromide	3.45	2.18	3.50[n]	4.18	3.42	3.82	3.47	22	6	55	39
82[c]	9-anthracenemethanol	2.34[k]	−0.42	3.04	3.21[o]	3.18	3.50[r]	3.32	8	18	77	5
83	acetophenone	1.14[i]	0.62	1.58	1.73	2.08	2.01	2.21	14	75	20	5
84	aniline	−0.10[k]	−0.52	0.90	2.32[o]	1.99	1.63[q]	2.13	12	87	13	0
85	anisole	2.09[i]	1.44	2.11	2.30	2.26	2.31	2.35	14	59	14	27
86	anthracene	4.20[i]	2.53	4.45	4.08[o]	4.03		4.06	13	2	47	51
87	benzaldehyde	1.06[i]	0.79	1.48	1.80	1.96		2.09	12	88	7	5
88	benzene	2.15[i]	1.27	2.13	2.43[o]	2.31	2.10	2.39	5	60	12	27
89	benzylalcohol	−0.43[i]	−1.18	1.10	1.85	2.24	2.03	2.38	14	57	43	0
90	biphenyl	4.08[i]	2.32	4.01	3.61[o]	3.80		3.78	7	4	21	75
91	bisphenol A	−0.91	−2.70	3.32	2.87	2.24	2.95	2.39	10	94	6	0
92	chlorobenzene	2.84[i]	2.74	2.89	3.15[o]	2.77	2.81[q]	2.81	12	16	37	47
93	dibutyl phthalate	4.32	5.24	4.72	3.54	4.00		3.97	13	1	19	81
94[c]	ethanol	−2.19[i]	−2.08	−0.31	1.81	1.81	1.96[s]	1.96	4	99	1	0
95	ethylnicotinate	0.55[k]	0.27	1.32	1.79	1.97	1.91	2.11	16	85	14	2
96	fluoranthene	5.00	2.75	5.16	4.93	4.66		4.64	12	1	24	75
97	methyl-4-chloro-2-nitrobenzoate	0.95	0.98	2.38[n]	2.13	1.88	2.27	2.01	12	91	4	5
98	methyl-4-nitrobenzoate	0.63	0.90	1.85[n]	2.26	1.82		1.96	12	92	5	3
99	methylbenzoate	1.56[i]	1.81	2.12	1.88	1.96		2.07	14	71	13	16
100	N,N-dimethylaniline	2.17	1.20	2.31	2.03	2.48	2.78	2.57	14	41	40	19
101	n-propylbenzene	3.84	2.98	3.72	3.72	3.64	3.29	3.65	16	3	37	59
102	naphthalene	3.41[i]	1.90	3.30	3.19[o]	3.22		3.22	9	12	26	62
103	nitrobenzene	1.47[k]	0.77	1.85	1.80[o]	2.18	2.01[q]	2.30	12	67	26	8
104	phenanthrene	4.74	2.53	4.46	4.28[p]	4.41		4.38	11	1	20	79
105	phenol	−1.08[i]	−1.68	1.47	1.71	2.04	1.87	2.18	12	84	16	0
106	pyridine	−0.45[k]	−0.89	0.65	1.89	1.98	1.86[s]	2.12	11	89	11	0
107	toluene	2.76[i]	1.93	2.73	2.43[o]	2.68	2.56	2.71	12	28	23	49

[a]Estimated by the fragment method,[97] if not marked otherwise. [b]Measured by us and published,[55] if not marked otherwise. [c]Experimental values from the ClogP database,[119] if not marked otherwise. [d]Measured in this study, if not marked otherwise. [e]Predicted values from the present model-logarithmized eq 10 combined with eq 11, with the coefficient values given in the last line of Table 3. [f]Measured in this study by isothermal titration calorimetry (ITC) incorporation method,[102] if not marked otherwise. [g]Number of possible poses at the interface. [h]Fraction of the bilayer amount in headgroups (H), at interface (I), and in core (C). More details in Table S1 in the Supporting Information. [i]Experimental values published.[120] [j]Published.[111] [k]Measured by us and published.[97] [l]Estimated by fragment method.[55] [m]Measured by us and published.[54] [n]Estimated by the ClogP approach.[119] [o]Measured by us and published.[98] Estimated values from this reference are not used. [p]Measured in this study and supersedes the published measured or estimated value.[98] [q]Published values for polychlorinated biphenyls (PCB)[57] and for other compounds.[107] [r]Measured by us using the ITC incorporation method and published.[98] [s]Measured in this study using the ITC solvent null method.[104]

DMPC (Avanti Polar Lipids, Alabaster, AL) was hydrated in borate buffer (5 mM $Na_2B_4O_7$, 180 mM H_3BO_3, and 18 mM NaCl, pH = 7.4) for 48 h at 37 °C with occasional vortexing. The suspension was extruded for 29 times to achieve even distribution of vesicle sizes. After extrusion, the exact DMPC concentration was determined using phosphate assay.[100]

Isothermal Titration Calorimetry (ITC) Measurement of Partitioning of Chemicals to Liposomes. The DMPC bilayer/water partition coefficients in liposome suspensions were measured using the VP calorimeter (MicroCal, Northampton, MA). The calorimeter cell has a volume of 1.4347 mL, and the syringe has a volume of 294.26 μL. Before loading in the cell, all solutions were subjected to 10 min degassing in order to get rid of the air bubbles, which may cause errors in the solution volume in the cell. The temperature of all used solutions was kept at 37 °C, i.e., above the main transition temperature of DMPC, in order to keep the bilayer in the fluid state. A stirring speed of 310 rpm was set for all the experiments. MicroCal Origin software was used to perform all the fitting procedures.[101]

The setup of the experiments was chosen to maximize precision. On the basis of the affinities of the tested chemicals for the bilayer, two different setups were used: the incorporation protocol and the solvent null approach.

Incorporation Protocol. This method,[102] using the titration of the solution of the chemicals by the liposome suspension, was used to determine the bilayer/water partition coefficients for the majority of the studied chemicals. The suspension of DMPC liposomes was loaded in the syringe, and the cell was filled with the solution of the chemical in borate buffer (pH 7.4). Liposome suspension was injected in the aliquots of 5 or 10 μL. For each compound, three background titrations were performed: (1) the buffer into the solution of the chemical to account for the heat of dilution and to confirm the absence of self-association of the chemical, (2) liposome suspension into the buffer to account for heat of dilution of the lipid, and (3) the buffer into the buffer to account for apparent heat caused by possible small differences between the temperatures of the solutions in cell and in syringe.

The corresponding heat generated after the ith injection, δh_i, can be expressed as

$$\delta h_i = c_D \Delta H_D^{w \to b} V_{cell} \frac{K}{(1 + iK\delta c_L)} \delta c_L \tag{2}$$

where c_D is the concentration of the chemical in the cell after the ith injection, $\Delta H_D^{w \to b}$ is the transfer enthalpy of the chemical from the aqueous phase to the bilayer, K is the mole-ratio partition coefficient, δc_L is the increase of the lipid concentration in the cell due to each injection of lipid suspension, and V_{cell} is the volume of the cell. Two parameters, $\Delta H_D^{w \to b}$ and K, were optimized by the fit of eq 2 to experimental data. The mole-ratio partition coefficient, K, was then converted to molarity-based partition coefficient, P, using

$$P = \frac{c_b}{c_w} = \frac{K(1 + Kc_L)}{1 + K(c_L + c_D)} \frac{n_L(V_{cell} - V_b)}{V_{cell}V_b} \tag{3}$$

assuming that the concentrations of the chemical in the bilayer (c_b) and aqueous phase (c_w) are both sufficiently low to approximate activities. The subscripts D and L indicate total concentrations (c) or amounts (n) of the chemical and lipid, respectively. The density of the DMPC in liposomes[103] of ~1 g/mL was used to calculate the bilayer volume (V_b).

Solvent Null Protocol. This method[104] uses the titration of the solutions of the chemical with different concentrations by the equilibrated mixture of the liposomes with the chemical. If the chemical concentration in the calorimeter cell does not match the free concentration of the chemical in the suspension loaded in the syringe, heat will be either absorbed or released upon mixing. No heat will be generated only when the concentration in the cell is equal to the free concentration in the suspension. This so-called solvent null concentration is used to calculate the actual amount of the chemical bound to lipid.

The solvent null method was applied to those chemicals that have very low partition coefficients so that the curvature of the δh_i plots in the incorporation protocol was insufficient to allow for a good fit by eq 2. Aliquots of 10 μL DMPC liposome chemical-buffer suspension were injected to various concentrations of chemical solutions in borate buffer (pH 7.4) loaded in the cell. Before loading, the liposome suspension was combined with the solution of the chemical at room temperature, and the mixture was incubated at 37 °C for 1 h. For each experiment, the corresponding controls were performed: (1) the chemical in the null concentration titrated into all concentrations of the chemical in the cell; and (2) the neat lipid titrated into buffer. The molarity-based partition coefficient, P, was calculated as

$$P = \frac{(n_0 - n_f)(V_{cell} - V_b)}{n_f V_b} \tag{4}$$

where n_0 is the amount of the chemical mixed with the liposome suspension; n_f is the free amount determined through the null concentration, and V_b and V_{cell} represent the volumes of the bilayer and the cell, as defined previously.

Modeling Drug Distribution in Bilayer Strata. Experimental information about overall partitioning of drugs into PC monolayers or bilayers can be conveniently obtained using common analytical techniques, some of which are described above. The measurements can be made directly on the suspension of monolayer particles or liposomes in equilibrated drug solution (by UV–Vis difference spectroscopy,[105] isothermal titration calorimetry,[102,104] and pH-metric titration for ionizable drugs[106]) or, alternatively, on the equilibrated drug solution after separation of liposomes or monolayer particles. The molarity-based partition coefficients (P) between the PC phase and water are calculated using the estimated volumes of monolayer or bilayer PC phases.

The partitioning of a compound into the PC monolayer or bilayer comprises its accumulation in the H- and C-strata, and the interface between them. The accumulation at the interface can be described using the surface-based interface/water equilibrium constant $S_{i/w}$ (dimension 1/length), representing the ratio of the surface concentration s_i (per unit area) and the aqueous concentration. The surface of the interface is practically equal to the surface of the H-stratum (A_h) because of the small thickness (h_h) of the H-stratum as compared to the curvature radius of the liposome or the particle. The drug amount at the interface is $n_i = s_i A_h = c_i V_h$. The second equality comes from the conversion of the surface-based concentration to the volume-based concentration, with the reference to the H-stratum volume. This step needs to be done because the fragment solvation energies, which will be used to describe the interface partitioning, are given for the volume-based concentrations, and the volumes are used to express the drug

amounts in the H- and C-strata. The relationship between the surface-based equilibrium constant $S_{i/w}$ and the volume-based partition coefficients $P_{i/w} = c_i/c_w$ is

$$S_{i/w} = \frac{s_i}{c_w} = \frac{c_i V_h / A_h}{c_w} = P_{i/w}\frac{V_h}{A_h} = P_{i/w}h_h \quad (5)$$

The partition coefficients (P) values for the entire monolayer or bilayer can be expressed as the ratio of drug concentration in the PC phase and water:

$$P_{x/w} = \frac{c_x}{c_w} = \frac{c_h V_{hx} + c_c V_{cx} + c_i V_{hx}}{V_x c_w}$$
$$= P_{h/w}\frac{V_{hx}}{V_x} + P_{c/w}\frac{V_{cx}}{V_x} + P_{i/w}\frac{V_{hx}}{V_x} \quad (6)$$

where c are the concentrations, and V are the volumes. The subscripts x, w, h, c, and i denote the entire monolayer or bilayer (x = m or b, respectively), the aqueous phase including the internal aqueous phase of liposomes, the H-stratum, the hydrocarbon C-stratum, and the H/C interface, respectively. The interface/water partitioning is characterized by a concentration-based partition coefficient, with the concentration of the interface-bound species expressed with regard to the headgroups' volume, to maintain consistency with the descriptions of the other two partitioning processes.

The surrogate phases for the H- and C-strata are introduced into the model using the Collander eq 1. The core is imitated by the C16 phase. The surrogate partition coefficient for the headgroups, $P_{DacPC/W}$, cannot be measured directly but can be calculated as the ratio of two other partition coefficients:

$$P_{x/w} = \alpha_h\left(\frac{P_{C16/W}}{P_{C16/DAcPC}}\right)^{\beta_h}\frac{V_{hx}}{V_x} + \alpha_c P_{C16/W}^{\beta_c}\frac{V_{cx}}{V_x} + P_{i/w}\frac{V_{hx}}{V_x} \quad (7)$$

The regression coefficients α and β have different values for the H-stratum, the C-stratum, and the H/C interface, the latter expressed using eq 8 (subscripts h, c, and i, respectively).

Various poses (orientations) of a compound at the H/C interface may contribute to the observed $P_{i/w}$ value:

$$P_{i/w} = \frac{c_i}{c_w} = \frac{\sum_{\text{poses } j} c_{ij}}{c_W} = \sum_{\text{poses } j} P_{ij}$$
$$= \alpha_i \sum_{\text{poses } j} 10^{\beta_i(\sum_{\text{H-location k}} f_{ijk} + \sum_{\text{C-location k}} f_{ijk})} \quad (8)$$

Here, the subscripts ij mark the volume-based interface concentration (c_{ij}) and the partition coefficient P_{ij} of the jth pose at the interface. The P_{ij} is defined using two sums of the logP-related fragment solvation characteristics: one using the DAcPC/W characteristics for the fragments located in the H-stratum and the other using the C16/W characteristics for the fragments located in the C-stratum.

■ RESULTS

The data set assembled for testing the hypothesis about estimating drug distribution in bilayer strata from modeling overall bilayer partitioning data is presented in Table 1. For 107 compounds, there are 95 $P_{m/w}$ values for the monolayer partitioning and 63 $P_{b/w}$ values for the bilayer partitioning. The $P_{m/w}$ and $P_{b/w}$ values for the same compound, where available, do not differ much because the headgroup and core phases of

monolayers and bilayers behave in similar way, and the difference is only caused by the volumes of the two strata. The published $logP_{b/w}$ were measured in unilamellar DMPC liposomes[57,107] at 35−37 °C. Other published DMPC partitioning data were not used because either the experiment temperature[108−113] was too close to the DMPC gel−fluid transition temperature (24 °C)[114] or the compound characteristics for eqs 10 and 11 below were missing.[42,115−117] The used compounds either cannot ionize in water or have negligible ionization in the used medium with pH = 7.4, i.e., the bases have $pK_a \leq 5.4$ and the acids have $pK_a \geq 9.4$ (estimated by ACD Percepta,[118] see Table S2 in Supporting Information). Most C16/W and all C16/DAcPC partition coefficients were either measured in our lab or estimated using the solvation characteristics for fragments obtained using the ClogP fragmentation scheme,[35] which we published previously.[55,97] Bilayer partitioning data were measured in DMPC liposomes by us or others, and in DMPC monolayers adsorbed on octadecylated nonporous silica microspheres by us. All available data are included in Table 1. Some of the data from our laboratory were previously published. Some predictions from the calibrated model, the partition coefficients and the intrabilayer distribution, are also listed in Table 1.

For individual variables in Table 1, the minimum and maximum values, the average, and the standard deviation are −3.34, 7.25, 3.16, and 2.49 for $logP_{C16/W}$; −3.04, 10.37, 2.62, and 2.85 for $logP_{C16/DAcPC}$; −3.12, 2.76, 0.54, and 1.02 for $logP_{DAcPC/W}$ (calculated as $logP_{C16/W} - logP_{C16/DAcPC}$, used in the model but not shown in Table 1); −0.31, 8.16, 3.88, and 1.93 for $logP_{O/W}$; 1.67, 6.91, 3.51, and 1.35 for $logP_{m/w}$; 1.41, 6.33, 3.25, and 1.36 for $logP_{b/w}$.

Distributions for all variables are shown in Figure 1. Only the $logP_{C16/DAcPC}$ values exhibit normal distribution at the 0.05
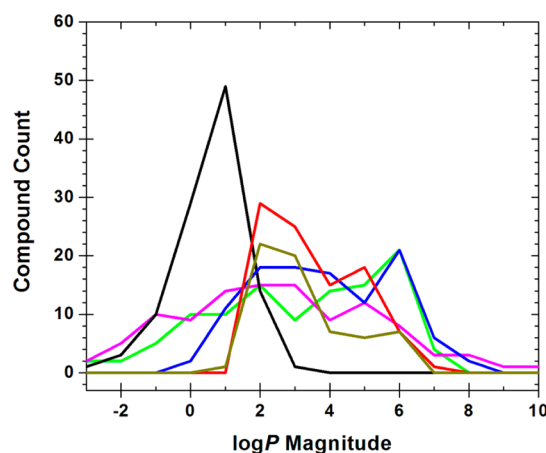
Figure 1. Distribution of independent variables ($logP_{C16/W}$, green; $logP_{C16/DAcPC}$, magenta; $logP_{DAcPC/W}$, black; $logP_{O/W}$, blue) and dependent variables ($logP_{m/w}$, red; $logP_{b/w}$, brown) (Table 1). The bins are one unit wide and centered at the integer logP magnitudes.

probability according to the Shapiro−Wilk test,[101] although the deviations from normality for other variables are not dramatic. The distributions for the C16/W and O/W partition coefficients are slightly skewed because of a number of nonpolar aromatic molecules, which have the logP values of ~6. These compounds have lower partition coefficients in the C16/DAcPC system thanks to the interactions of aromatic rings with DAcPC, and this fact keeps the C16/DAcPC

distribution normal. The calculated values for the DAcPC/W system continuously rise to a sharp maximum at $\log P_{DAcPC/W} = 1$ but then exhibit a fast decline leading to a slightly asymmetrical distribution. The maximum $\log P_{DAcPC/W} = 1 \pm 0.5$ comprises about a half of the studied set. In contrast to the other two solvent/water systems, the $\log P_{O/W}$ values lack the negative values because of a higher partitioning of hydrophilic compounds in 1-octanol than in nonpolar solvents thanks to the high water content and H-bonding in 1-octanol. The monolayer and bilayer data show incomplete normal distributions; they lack the lower $\log P$ values, which are difficult to measure. For the solvent/water systems, the low $\log P$ measurements can be performed using varying volume ratio of the used phases.

Model of Drug Distribution in Bilayer. The concentration-based, overall partition coefficient (P) between the entire monolayer or bilayer (subscript x = m or b, respectively) and water (subscript w) is described as a weighted sum of the partition coefficients in individual strata (H-stratum − headgroups, C-stratum − core, and H/C interface denoted by subscripts h, c, and i, respectively), where the weights are relative volumes of the H- and C-strata (see eq 6 for details):

$$P_{x/w} = P_{h/w} \frac{V_{hx}}{V_x} + P_{c/w} \frac{V_{cx}}{V_x} + P_{i/w} \frac{V_{hx}}{V_x} \quad (9)$$

Here, V are the volumes of the phases indicated by the subscripts. The interface/water partitioning is characterized by a concentration-based partition coefficient ($P_{i/w}$), with the concentration of the interface-bound species expressed with regard to the headgroups' volume, to maintain consistency with the descriptions of the other two partitioning processes, and to account for the double interface area of the bilayer as compared to the monolayer. This description is permissible as long as the surface density of the interface-bound molecules is sufficiently low to ensure independent binding. More details are provided in the text accompanying eq 6.

Using the Collander equation (eq 1), the surrogate phases for the H- and C-strata are introduced into eq 9. The headgroups are imitated by the hydrated DAcPC phase and the core by the C16 phase:

$$P_{x/w} = \alpha_h P_{DAcPC/W}^{\beta_h} \frac{V_{hx}}{V_x} + \alpha_c P_{C16/W}^{\beta_c} \frac{V_{cx}}{V_x} + P_{i/w} \frac{V_{hx}}{V_x} \quad (10)$$

The surrogate partition coefficient for the headgroups is calculated as $P_{DAcPC/W} = P_{C16/W}/P_{C16/DAcPC}$. Compounds may interact with the H/C interface in various poses (orientations, conformations, and positions). Therefore, the observed $P_{i/w}$ value in eq 10 is expressed as the sum of the partition coefficients for each of the poses (see eq 8 for more details):

$$P_{i/w} = \sum_{poses\,j} P_{ij} = \alpha_i \sum_{poses\,j} 10^{\beta_i \log P_f}$$

$$= \alpha_i \sum_{poses\,j} 10^{\beta_i (\sum_{H-location\,k} f_{ijk} + \sum_{C-location\,l} f_{ijl})} \quad (11)$$

The subscript ij indicates the relationship to the jth pose at the interface. The partition coefficient (P_{ij}) for each pose is defined as the partition coefficient obtained from fragments (P_f), scaled by the Collander coefficients as in eq 1. Each $\log P_f$ value is generated using two sums of the $\log P$-related fragment solvation characteristics (f, summarized in Table 2), which were determined previously for the fragmentation used in the

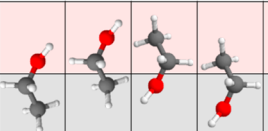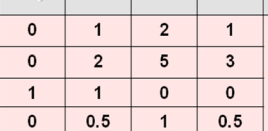**Table 2. Fragment Solvation Characteristics for C16/DAcPC, C16/W, and DAcPC/W Systems**

fragment		fragment solvation parameters		
symbol	full name	C16/DAcPC[a]	C16/W[b]	DAcPC/W[c]
Ca	aromatic [a] isolating carbon	0.084	0.077	−0.007
CA	aliphatic [A] isolating carbon	0.336	0.108	−0.228
H	hydrogen on isolating carbon	0.134	0.287	0.153
OHa	hydroxyl [a]	−2.651	−2.788	−0.137
OHA	hydroxyl [A]	−2.788	−3.656	−0.868
OHZ	hydroxyl [Z]	−2.976	−2.967	0.009
OAa	ether [Aa]	−0.106	−0.955	−0.849
EsAa	ester [Aa]	−0.144	−1.299	−1.155
Ala	aldehyde [a]	−0.283	−1.052	−0.769
COAa	carbonyl [Aa]	−1.278	−1.774	−0.496
COaa	carbonyl [aa]	−0.096	−1.562	−1.466
NH2a	primary amine [a]	−1.866	−2.166	−0.300
NAAa	tertiary amine [AAa]	−0.646	−1.120	−0.474
NO2a	nitro [a]	−0.768	−0.592	0.176
Naraa	aromatic nitrogen [aa]	−1.340	−1.611	−0.271
Cla	chloride [a]	0.698	1.078	0.380
Bra	bromide [a]	1.401	1.096	−0.305
BrA	bromide [A]	−0.247	0.069	0.316
Correction Factors				
BB	benzyl bond to simple aromates	0.139	−0.177	−0.316
Chain	chain	−0.197	−0.057	0.140
CHBr	chain and cluster branch	−0.290	−0.125	0.165
FAC	extended aromatic iso-C	0.001	0.149	0.148
HB	pair-H bond	0.627	1.323	0.696
NOrtho1[d]	ortho substitution 1	0.038	0.147	0.109
NOrtho2[d]	ortho substitution 2	0.436	−0.476	−0.912
NOrtho3[d]	ortho substitution 3	0.3103	−0.27	−0.580
PCCY	phenyl-fragment pair	−0.065	0.244	0.309
PIWR1[e]	potential interaction within ring 1	−0.52	0.092	0.612
PIWR2[e]	potential interaction within ring 2	−0.632	0.114	0.746
PIWR3	potential interaction within ring 3	−0.211	0.370	0.581

[a]Published.[97] [b]Published.[55] [c]Calculated as the difference between the C16/W and C16/DAcPC values. [d]For the interacting fragments with the $f > -0.12$ (Northo1), $-0.25 \leq f \leq -0.12$ (Northo2), and $f < -0.25$ (Northo3). The average is used if the f values are from different categories.[97] [e]For the interacting fragments with the $f < 0.15$ (PIWR1), $0.15 \leq f \leq 0.5$ (PIWR2), and $f > 0.5$ (PIWR3). The average is used if the f values are from different intervals.[97]

ClogP system[35] by regression analysis of the DAcPC/W and C16/W partition coefficients.[55,97] In the first sum (k-summation), the DAcPC/W characteristics are used for the fragments interacting with the headgroups (H-location). The second sum (l-summation) contains the C16/W characteristics for the fragments located in the core (C-location). The interfacial poses exhibit the Boltzmann distribution, with the fraction of the jth pose being equal to $P_{ij}/\Sigma P_{ij}$.

Individual poses were created for each compound using the following algorithm, illustrated for ethanol (**94**, Table 1) in Figure 2: (1) generate the most extended conformation; (2)

Figure 2. Set of generated interface poses for ethanol (94). Individual $\log P_f$ values, used in eq 11, are obtained by summing up the fragment solvation characteristics (Table 2) for the phase, where the fragment is located. The chain factor, correcting for the chain length, was scaled based upon the location of the two carbons forming the chain. This principle was applied to other correction factors, which are applied to a larger substructure: they were composed of the contributions from each phase, sized by the proportion of the substructure present in the given phase.

orient the molecule in this conformation so that its long axis is parallel to the bilayer normal, to minimize bilayer disturbance as observed in MD simulations;[89,121] (3) create individual poses by moving the oriented molecule from one phase to the opposite phase across the H/C-interface in small, preferably atom-by-atom, steps leading to different numbers of atoms in the H- and C-strata; and (4) repeat step 3 with inverted molecule, so that both possible orientations along the long axis are examined. If a molecule cannot adopt a clearly prolonged shape, and the long axis is not significantly longer than other axes, repeat steps 2−4 also for the axis perpendicular to the long axis.

The model represented by logarithmized eq 10 combined with eq 11 was calibrated by nonlinear regression analysis[122] based on experimental data ($P_{m/w}$ and $P_{b/w}$ in Table 1) using the independent variables $P_{DAcPC/W} = P_{C16/W}/P_{C16/DAcPC}$ and $P_{C16/W}$ (Table 1) and f (Table 2). The regression coefficients α and β may have different values for the H- and C-strata and the H/C interface (subscripts h, c, and i, respectively). On the basis of the experimental data[48] and molecular dynamics simulations,[123] the volume ratio of both headgroup strata to the core in the DMPC bilayer was estimated as $V_{hb}/V_c = 7{:}13$ and the H/C volume ratio in monolayers was estimated as $V_{hm}/V_c = 1{:}3$. These volume ratios were kept fixed in the optimization process.

The optimized values of regression coefficients α and β for the fit of logarithmized eq 10 combined with eq 11 to experimental data given in Tables 1 and 2 are summarized in Table 3. The number of experimental data points was $n = 158$ in all cases.

Interestingly, even without calibration, the model explains 79% of experimental variance (line 1 in Table 3). This is a typical model quality for calibrated models based on frequently used topological descriptors, which often bear no physical relationship to the solvation process. Optimization of any pair of the Collander coefficients α and β (lines 2−4) enhances the fit, with most improvement seen for the optimized i/w coefficients leading to the squared correlation coefficient value of $r^2 = 0.913$ and a 35% reduction in the value of the standard deviation (SD = 0.392). When two pairs of the Collander coefficients are optimized (lines 5−7), the agreement with the experiment increases, up to $r^2 = 0.928$ and SD = 0.356 for the best combinations of the c/w and i/w coefficients. The best result, 94% of explained variance and SD = 0.324, is achieved when all six values of the α and β coefficients are optimized (line 8). Apparently, no reduction in the number of coefficients leads to a better fit, as indicated by the increasing F-test values (F). The standard errors of coefficients are acceptable, especially considering that all of them are nonlinear coefficients in the logarithmized eq 10 combined with eq 11.

Given the number of data points (158) and the number of optimized coefficients (6), there is low probability of a chance correlation. The stability of the correlation is confirmed by the cross-validation based on the omission of 21 (13.3%) data points at a time, which was repeated ten times. The omission of compounds was performed by a random selection of three compounds from each of the seven bins of about equal size for the data points ordered by the magnitude of the $P_{x/w}$ values (x = m or b), to ensure that the entire $P_{x/w}$ range is represented. This binning does not cluster similar compounds because the overall partitioning depends on the affinity for the H-, C-, and H/C strata, and a small structural change may cause a large change in the $P_{x/w}$ value. The average predictive squared correlation coefficient, $q^2 = 0.924$, corresponds well with $r^2 = 0.941$ for the full fit. The average predictive sum of squares of deviations PRESS = 2.315 leads to a value of the corresponding SD equivalent (~square root of 2.315/21) equal to 0.332, which is commensurate with the SD = 0.324 for the full training set.

The calibrated model, logarithmized eq 10 combined with eq 11, with the optimized coefficient values in the last line of Table 3, predicts the drug distribution in individual strata of the DMPC bilayer (Table 1, the last three columns, and Table 4). For the interfacial poses, more detailed characterization is provided in Figure 3 and Table S1 in Supporting Information,

Table 3. Regression Coefficients and Statistical Indices of Calibrated Model (eqs 10 and 11)

α_c	β_c	α_h	β_h	α_i	β_i	r^2	SD	F
1	1	1	1	1	1	0.792	0.607	149.38
4.229 ± 2.560	0.783 ± 0.059	1	1	1	1	0.821	0.563	173.60
1	1	209.3 ± 48.90	0.123 ± 0.108	1	1	0.893	0.436	289.96
1	1	1	1	21.37 ± 4.061	0.353 ± 0.048	0.913	0.392	357.94
1	1	265.7 ± 48.37	0.231 ± 0.078	0.768 ± 0.221	0.832 ± 0.170	0.924	0.366	410.13
0.741 ± 0.407	0.973 ± 0.045	1	1	20.71 ± 3.589	0.381 ± 0.043	0.928	0.356	434.52
0.222 ± 0.218	1.023 ± 0.073	225.308 ± 43.302	0.129 ± 0.088	1	1	0.924	0.368	407.23
0.954 ± 0.465	0.946 ± 0.039	272.0 ± 42.97	0.215 ± 0.069	0.551 ± 0.129	0.918 ± 0.129	0.941	0.324	523.22

Table 4. Predicted Bilayer Locations for Compounds with Known Bilayer Locations

		log P			bilayer/water			relative amount (%)[f,g]			
no.	compound	C16/W[a]	C16/DAcPC[b]	O/W[c]	exptl[d]	calcd	NP[e]	H	I	C	exp. location[g]
108	1-propanol	−1.53	−1.23	0.25		1.94	6	94	6	0	H
109	3-methylindole	0.81	0.88	2.17		2.11	14	71	26	3	H
110	9H-carbazole	2.21	0.74	3.06		2.64	10	45	37	18	H[i]
88[h]	benzene	2.15[a]	1.27[b]	2.13[c]	2.10	2.39	5	60	12	27	H
89[h]	benzylalcohol	−0.43[a]	−1.18[b]	1.10[c]	2.03	2.38	14	57	43	0	H
91[h]	bisphenol A	−0.91[a]	−2.70[b]	3.32[c]	2.95	2.39	10	94	6	0	H
94[h]	ethanol	−2.19[a]	−2.08[b]	−0.31[c]	1.96	1.96	4	99	1	0	H
111	indole	0.75	0.14	1.67		2.26	10	70	28	2	H
112	methanol	−2.77	−2.05	−0.77		1.83	2	100	0	0	H
106[h]	pyridine	−0.45[a]	−0.89[b]	0.65[c]	1.86	2.12	11	89	11	0	H
113	1-butanol	−0.81	−0.83	0.88		2.00	9	96	4	0	H/I[j]
114	1-pentanol	−0.81	−0.42	1.35		2.25	10	44	56	0	H/I[j]
82[h]	9-anthracenemethanol	2.34[a]	−0.42[b]	3.04[c]	3.50	3.32	8	18	77	5	I[k]
11[h]	1-hexanol	0.44[a]	−0.01[b]	2.03[c]	1.91	2.69	10	24	76	0	I
115	1-heptanol	1.06	0.39	2.41		3.19	14	9	91	0	I
116	1-octanol	1.69	0.80	2.94		3.74	16	3	97	0	I
117	4-tert-octylphenol	3.49	0.96	5.16		4.65	15	1	96	3	I
6[h]	1,4-dimethylbenzene	3.25[a]	2.59[b]	3.15[c]	2.98	2.98	7	14	9	77	C
118	1,6-diphenyl-1,3,5-hexatriene	5.83	4.25	5.64		5.44	17	0	27	73	C
119	1-methyl-4-(6-phenyl-1,3,5-hexatrien-1-yl)-benzene	6.33	4.93	6.14		5.95	30	0	32	68	C
120	9-methylanthracene	5.05	3.26	5.07		4.66	6	1	18	82	C
121	9-ethylanthracene	5.68	3.67	5.52		5.22	6	0	13	87	C
122	ethylbenzene	3.20	2.46	3.15		3.26	14	11	36	53	C
123	n-decane	7.01	4.74	5.98		6.45	9	0	7	93	C
124	n-hexane	4.49	3.11	3.90		4.06	5	2	8	90	C
101[h]	n-propylbenzene	3.84[a]	2.98[b]	3.72[c]	3.29	3.65	16	3	37	59	C
107[h]	toluene	2.76[a]	1.93[b]	2.73[c]	2.56	2.71	12	28	23	49	C

[a]Predicted values according to ref 97 except the marked values, which are listed in Table 1. [b]Predicted values according to ref 55 except the marked values, which are listed in Table 1. [c]Estimated by the ClogP approach[119] except the marked values, which are listed in Table 1. [d]Listed in Table 1. [e]Number of possible poses at the interface. [f]Fraction of the amount in the bilayer strata (total amount in the bilayer = 100%). [g]Headgroups, H; interface, I; core, C. [h]Listed in Table 1 and used in model calibration, which did not utilize the location information. [i]See Discussion. [j]Published as I only; see Discussion for explanation. [k]Published as H, but I is more plausible; see Discussion for explanation.
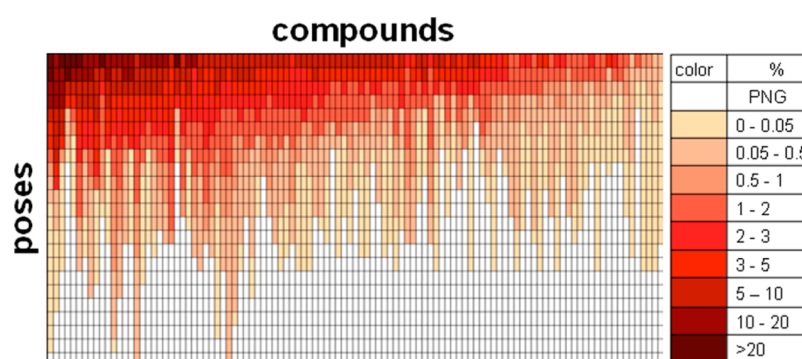
Figure 3. Distribution of the prevalences of interfacial poses of individual compounds predicted by the calibrated model. The poses were generated using the algorithm described in Figure 2 and the accompanying text. The compounds are arranged in the order of decreasing interface accumulation (left to right). The poses are listed in the order of decreasing prevalence. White color indicates the poses, which were not generated (PNG).

listing relative drug amounts in individual interfacial poses as well as in both H- and C-strata.

Inside the calibrated model, logarithmized eq 10 combined with eq 11, the sum of the P_{ij} values for individual poses is dominated by prevalent poses, and contributions of weak poses are marginalized. After calibration, individual P_{ij} values provide information about the prevalence of the given pose. Individual

poses for the used compounds are summarized in Table S1 in Supporting Information, along with the fraction of the compound present in each pose. The number of poses for each compound is also listed in Table 1. Inclusion of configurational entropy using the number of individual poses was attempted but did not lead to an improvement of the fit.

The number of considered poses for a compound increases with the length of the molecule in the extended conformation or with the absence of such conformation, when the poses along two axes need to be created. For individual compounds, 4−23 possible interfacial poses were generated, and all were simultaneously fed into the model. The distribution of predicted prevalences of poses for individual compounds is depicted in Figure 3. The model effectively reduces the number of considered poses. The number of significant poses (>2%) is four or less for 56 (52%) compounds. Note that the first three shades mark low, insignificant prevalences and are only shown to illustrate the numerical aspect of the approach. Figure 3 also shows that the number of considered poses does not vary substantially between compounds exhibiting a high preference for the interface and the rest of the compounds. Expected amphiphilicity of a compound, or the lack of thereof, is not considered in generating possible interfacial poses.

Model Validation. The presented model was calibrated using the overall partition coefficients and predicts, in addition to these characteristics, intrabilayer distribution. These latter predictions were chosen for independent validation of the model because they are more challenging than the overall partition coefficient (see Discussion). For several dozen compounds, the preferred locations in the fluid PC bilayer were experimentally determined, as summarized previously, along with the used techniques.[33] For all compounds, for which experimental or predicted independent variables ($P_{C16/W}$ and $P_{C16/DAcPC}$) and the fragment solvation characteristics (f) for both C16/W and C16/DAcPC systems were available, preferred locations are compared with predictions from our model (Table 3, the last line) in Table 4. Compounds with available $P_{b/w}$ values in Table 4 were included in the set used for model calibration (Table 1), but the information about the preferred location was not used in that process.

The validation data set is not trivial and the locations are in many cases hard to guess using standard chemical intuition. The preferred location depends on the character of fragments forming a molecule. Small aromates prefer the headgroups (benzene, **88**; pyridine, **106**), as do larger aromates containing heteroatoms (9*H*-carbazole, **110**; indole, **111**), contrary to the common perception that they should accumulate in the core because of high hydrophobicity as indicated by their O/W partition coefficients (Table 4). Aromates lose the preference for the headgroups by addition of alkyl substituents, as seen in toluene (**107**), ethylbenzene (**122**), *n*-propylbenzene (**101**), and 1,4-dimethylbenzene (**6**), or an alkenyl chain as in 1,6-diphenyl-1,3,5-hexatriene (**118**) and its methyl derivative (**119**). Naturally, alkanes such as *n*-hexane (**124**) and *n*-decane (**123**) then reside almost exclusively in the core. Halogenation of aromates increases their affinity for the core thanks to the positive values of the Cla and Bra fragment parameters listed in Table 2. A single hydroxyl group can pull a molecule from the core into the interface, as seen for the 9-methylantracene (**120**)/9-anthracenemethanol (**82**) pair, or even into headgroups, as illustrated by the toluene (**107**)/benzylalcohol (**89**) pair. However, there are no simple qualitative rules for estimation of preferred bilayer location, which is determined by a delicate balance of fragment solvation characteristics in the molecule. For instance, the addition of a single methyl group is sufficient to change the preference from the headgroups to the core for the benzene (**88**)/toluene (**107**) pair but not for the indole (**111**)/3-methylindole (**109**) pair.

The calibrated model faithfully captures this complex behavior (Table 4). The agreement between the model predictions and experimental data is very good taking into account that the experimentally determined preferred location means prevalent but not exclusive accumulation in that location. Only for two (1-butanol, **113**; 1-pentanol, **114**) out of 27 compounds are the experimentally determined preferred locations different from the prevalent location indicated by the model, and the experimental data are not definite in these two cases (see Discussion). The experimentally determined preferred strata have more than 50% and often significantly higher prevalence predicted in all cases except 9*H*-carbazole (**110**), which is still predicted correctly as having the highest accumulation in the headgroups.

■ DISCUSSION

The presented approach to prediction of the bilayer distribution of compounds is unique thanks to the use of hydrated DAcPC as the H-stratum surrogate. Solvatochromic analysis[55] showed that the DAcPC phase, in comparison to bulk water, maintains higher H-bond acceptor ability but has diminished H-bond donor ability. These observations are contradictory to the often used assumption about similar solvation properties of the headgroup stratum and bulk water,[70,124−127] stemming from the high headgroup hydration.

The calibrated model (Table 3, the last line) describes well the overall partition coefficients of 107 compounds, which do not ionize under experimental conditions. Extensive cross-validation shows that the model is stable and predictive. The Collander coefficients have the optimized values close to unity for the core (both α_c and β_c) and the H/C interface (β_i only), indicating high similarity and collinearity, respectively, between the natural and surrogate partition coefficients. For headgroups, there is a significantly nonlinear relationship between the natural and surrogate partition coefficients, described by the low β_h value, which is compensated by the high α_h value. This fact could indicate that the Collander coefficients for headgroups account for some phenomena, which were not included in the model, e.g., electrostatic interactions, entropy changes, and/or cavity creation (although the latter aspect is partially covered by the fragment solvation characteristics).

Interpretation of Some Model Validation Data. Experimentally determined preferred locations of 27 compounds were used for independent validation of the model. The preferred location was predicted correctly for 25 compounds, and the experimental data were not conclusive for the remaining two compounds, **113** and **114** (Table 4). Two more compounds, **82** and **110** (Tables 1 and 4), also deserve some discussion.

The preferred location of 9-anthracenemethanol (**82**) was determined by the parallax analysis, which uses fluorescence quenching fragments covalently bound at different positions along the PC molecule.[32,128] The method does not provide much structural detail and places the center of the molecule at the extrapolated peak quenching depth. In the published pose, with the long axis perpendicular to the bilayer normal, the molecule of **82** is located at and above the ester groups of fatty acids, a position qualifying for the headgroup location. The published pose, however, does not minimize the disturbance of the interface and is therefore less probable than a pose with the long axis parallel to the bilayer normal, as observed in MD simulations for other compounds.[89,121] In the more probable pose, the atoms of one of the outer rings would reach into the

core, and the pose would be classified as amphiphilic, in contrast to our previous assessment,[33] which used the conclusion about the headgroup location made in the original studies.[32,128] As seen in Table 4, our model prefers the interface location (74%), along with some headgroup accumulation (20%).

The 9H-carbazole (**110**) is the only correctly predicted compound where the predicted prevalence did not exceed 50%. Location of **110** in the bilayer was also determined by the parallax analysis[128,129] as being about 3 Å closer to the headgroups than that of **82**. By applying the same considerations as for **82** in the preceding paragraph, **110** with the long axis parallel to the bilayer normal would be classified, in accordance with the model prediction (Table 4), as a cephalophile (predicted prevalence 44%), being very close to the interface (predicted prevalence 36%).

For n-alkanols, the preferred accumulation in headgroups was determined independently for ethanol (**94**).[130] It can be expected that with the chain elongation, n-alkanols become more amphiphilic, and at some point, the interactions with the interface prevail. There are two reports pinpointing the chain length when this change happens in 1-palmitoyl-2-oleoyl-PC vesicles. The lifetime and intensity ratios of fluorescence probes in the presence of n-alkanols indicated that the first three congeners (**112**, **94**, and **108**) prefer headgroups and that longer congeners (**113**, **114**, **11**, **115**, **116**) accumulate at the interface.[131] Photolysis of rhodopsin, an integral membrane GPCR protein, in the presence of n-alkanols placed the break point in the series on 1-hexanol (**11**), for which the effect was negligible, while a promoting effect was observed for shorter n-alkanols (**112**, **94**, **108**, **113**, and **114**), and an inhibitory effect was seen for longer n-alkanols (**115** and **116**).[132] Our model captures the transition from the headgroup preference to the interface preference with the alkyl chain extension but puts the transition point on 1-pentanol (**114**), i.e., between the outcomes of the two studies.

Predicted Distribution in Bilayer Strata. The calibrated model, logarithmized eq 10 combined with eq 11, with the optimized coefficient values given in the last line of Table 3, provides a prediction of drug distribution in individual strata of the DMPC bilayer for the compounds, for which the input data, the C16/W and the C16/DAcPC partition coefficients, and fragment solvation characteristics (Table 2) are available. The interfacial poses are generated using the algorithm described in Figure 2 and the accompanying text. The fragment-based partition coefficients of individual poses, P_{ij}, are calculated (eq 11) using the fragment solvation characteristics f in the DAcPC/W and C16/W systems for the fragments embedded in the headgroups and the core, respectively. The interfacial poses exhibit the Boltzmann distribution, with the fraction of the jth orientation being equal to $P_{ij}/\Sigma P_{ij}$.

The predicted values of relative drug amount in the headgroups, core, and at the interface (Tables 1 and 4) are plotted against the C16/DAcPC partition coefficients in Figure 4. The sigmoidal dependences marking, for the majority of compounds, the maximum fraction in the H- and C-strata can be discerned. The sigmoidal function for the H-stratum (FH, in %) as dependent on the respective logP values (the red line in Figure 4) is based on the definition of the C/H partition coefficient:[55]

$$FH = \frac{100}{\alpha P_{C16/DAcPC}^{\beta} + 1} \tag{12}$$
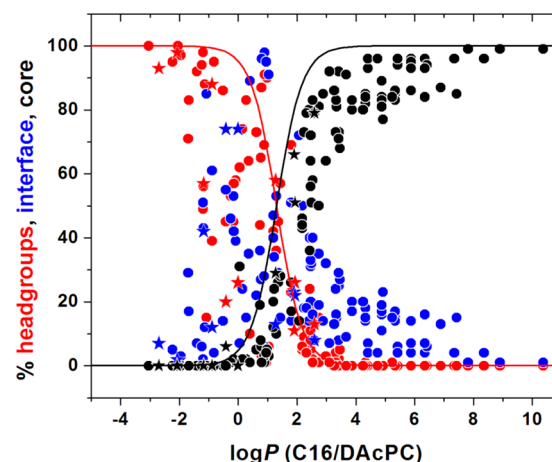
Figure 4. Relative amounts accumulated in headgroups, core, and the headgroups/core interface (red, black, and blue points, respectively) plotted against the C16/DAcPC partition coefficients (Tables 1 and 4). Points represent the predicted values, and stars mark the compounds with known bilayer location. The lines (see text for the equations) indicate the maximum fraction in the headgroup and core strata (red and black, respectively) attainable for the given P value.

The exponent β was added to account for a different composition of the bilayer strata and the surrogate systems using the Collander equation,[133] but it was not necessary because its value could be kept fixed as $\beta = 1$. The fraction in the C-stratum is, obviously, equal to $100 - FH$ (the black line in Figure 4). The functions adopt reasonable shapes if the coefficient is set to $\alpha = 0.05$.

As seen in Figure 4, the $P_{C16/DAcPC}$ value alone has a limited use as a predictor of bilayer location; it seems to only recognize cephalophiles having almost 100% accumulation in the H-stratum as compounds with the $logP_{C16/DAcPC} < -3$. Lipophiles with $logP_{C16/DAcPC} > 3$ prefer to accumulate in the C-stratum but also exhibit a minor but significant (up to 30%) adsorption at the interface, probably because of the aromatic character of the used lipophilic compounds. The compounds with $-3 < logP_{C16/DAcPC} < 3$ show widely varying distributions between individual bilayer strata. The asymmetric peak of blue points marking the interface accumulation starts rising at $logP_{C16/DAcPC} = -3$, reaches the expected maximum for $0 < logP_{C16/DAcPC} < 1$, but then decreases slowly, forming a long shoulder with the prevalence around 20% for up to $logP_{C16/DAcPC} \approx 8$. This shoulder contains a significant number of halogenated aromatics.

For several compounds, the prediction of the overall bilayer distribution, including the significant interfacial poses, is depicted in Figure 5. The shown molecular geometries and orientations approximate real interfacial poses, while absolutely no geometry or orientation is specified for the molecules accumulated in the H- and C-strata. The relative amounts in Figure 5 represent fractions of the total amount present in the bilayer. These bilayer amounts differ for individual compounds, if they are added to a bilayer/water system in equal doses. Drug distribution between the bilayer and aqueous phases can be calculated using the $P_{b/w}$ values in Tables 1 and 4 and assuming no protein binding. Using a realistic estimate for muscles, liver, and heart,[14,15] the volume of bilayers represents 2.5% of the total tissue volume. Then, the fractions of the total amount in the tissue that are present in the bilayer are 81% for indole (**111**, Figure 5A); 68% for 1-hexanol (**11**, B); 99% for 9-
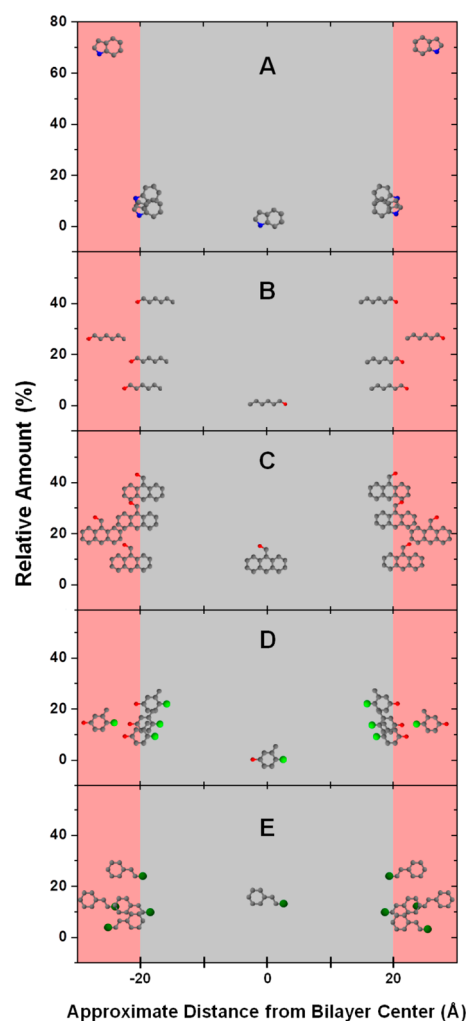
Figure 5. Predicted fraction (%) of the overall bilayer amount accumulated in the headgroup and core strata (pink and gray areas, respectively) and at the interface of the fluid PC bilayer for: A, indole (**111**); B, 1-hexanol (**11**); C, 9-anthracenemethanol (**82**); D, 4-chloro-3-methylphenol (**74**, one interface pose with prevalence of 16% is omitted for clarity); E, 1-bromo-2-phenylethane (**7**). The shown interfacial poses coarsely correspond to expected experimental poses.

anthracenemethanol (**82**, C); 97% for 4-chloro-3-methylphenol (**74**, D); and 93% for 1-bromo-2-phenylethane (**7**, E).

For indole (**111**, Table 4 and Figure 5A), peculiar experimental data are available showing bimodal distribution, with predominant binding to the headgroup phosphates but also some adsorption to the H/C-interface.[134] Interestingly, the presented approach is able to capture both headgroup accumulation and interfacial poses, which are very close to observed positions, and even approximate their prevalences (70% and 28%, respectively, Table 4), if all interfacial poses are lumped together. Figure 5B and 5C show well-separated prevalences for the H-stratum accumulation, three interfacial poses, and low core partitioning, which are predicted for 1-hexanol and 9-anthracenemethanol (**11** and **82**, Table 4), respectively. The predictions are in good agreement with experimental data, classifying these compounds as amphiphilic (Table 4). A similar pattern holds for 4-chloro-3-methylphenol (**74**), as shown in Figure 5D, although this compound exhibits smaller differences in the preferences for the H-stratum accumulation and individual interfacial poses (one pose with

16% prevalence, Table S1 in Supporting Information, is omitted for clarity). For 1-bromo-2-phenylethane (**7**, Figure 5E), the bilayer prevalences are much more comparable than for the other shown compounds. Interestingly, the interfacial poses are not similar as in the previous cases. The pose with the lowest shown prevalence resides in the headgroups except the benzene ring end, in contrast to the higher ranked poses, which only have the bromine end interacting with the headgroups.

The importance of intramolecular fragment positions for amphiphilicity is nicely illustrated using 2-, 3-, and 4-nitroaniline (**61**, **64**, and **78**, respectively, Table 1), having the overall $\log P_{b/w}$ values in the same range (2.45, 2.11, and 2.01, respectively). However, their intrabilayer distribution is rather different: **64** and **78** partition almost completely to the headgroups, while **61** shows higher preference for the interface. This fact cannot be explained by the DAcPC/W partition coefficient ($=P_{16/W}/P_{16/DAcPC}$), which actually has a higher value for **61** than for **64**. All three compounds contain cephalophilic amino and nitro groups, with the C16/DAcPC fragment solvation parameters $f(NH_2) = -2.166$ and $f(NO_2) = -0.592$ (Table 2, the suffix a denotes an aromatic skeleton). While the ortho-derivative **61** can have both groups located in the headgroups and the rest of the molecule crossing the interface into the core resulting in the interface prevalence of 62%, this option is greatly diminished for the meta-derivative **64** (6%) and the para-derivative **78** (4%).

Intrabilayer Distribution: Comparison with Other Approaches. Numerous computational studies mostly focused on qualitative prediction of bilayer distribution for one or two compounds at a time. For a comparison with our very good model predictions (Table 4), we selected studies predicting the preferred location of several compounds.

A multistrata, continuum approach, PPM (Positioning of Proteins in Membranes), was also applied to bilayer partitioning of small molecules.[79] None of the six compounds with experimentally determined bilayer locations had the location reproduced correctly. These results are a bit surprising given the level of sophistication of the approach and can probably be improved by refocusing the approach on partitioning of small molecules.

Atomistic depth-constrained MD simulations with several all-atom and united-atom lipid force fields were compared for their ability to predict partition coefficients of 11 compounds (see below).[96] The preferred locations of individual molecules (Table S6, Supporting Information)[96] varied between force fields, indicating that this characteristic is more difficult to reproduce than the overall partition coefficient. Experimentally determined location data are only available for a few compounds. For 1-butanol (**113**, Table 4) preferring the headgroups[132] or the interface,[131] the free energy minimum was placed at 8.9−11.1 Å from the bilayer center by four of the five tested force fields, and only one force field provided the more realistic distance of 19.8 Å. Benzylalcohol (**89**, Tables 1 and 4) prefers the headgroups,[26] but all force fields placed the free energy minimum in the more ordered core portion at 8.9−11.1 Å from the bilayer center. For 1,4-dimethylbenzene (**6**, Tables 1 and 4) accumulating in the bilayer center,[135] two force fields made the correct prediction, and three force fields placed the free energy minimum in the more ordered portion of the core, 6.1−10.0 Å from the center.

The same study[96] also used a multistrata, continuum COSMOmic approach[74] to examine bilayer partitioning of 11 compounds. Predictions of the free energy minima for the three

Table 5. Overall Accumulation (log$P$) in the PC Systems Correlated with log$P_{O/W}$[a] and the Solvatochromic Parameters

PC system	coefficients						n	r^2	SD	F
	a	b	s	e	v	const.				
monolayer[a]	0.729 ± 0.020					0.882 ± 0.082	95	0.965	0.355	1339
bilayer[a]	0.654 ± 0.022					1.057 ± 0.086	63	0.966	0.351	895.2
monolayer	0.0651 ± 0.197	-2.665 ± 0.235	-0.642 ± 0.210	0.693 ± 0.149	2.443 ± 0.181	0.934 ± 0.158	95	0.934	0.346	262.5
bilayer	0.382 ± 0.220	-2.672 ± 0.277	-0.875 ± 0.230	0.754 ± 0.242	2.093 ± 0.244	1.444 ± 0.192	63	0.934	0.344	167.9

[a]For the correlation with log$P_{O/W}$ using logarithmized eq 1, a is the slope and const is the intercept.

compounds above (**6**, **89**, and **113**) did not agree with experimental data.

Overall Bilayer Partitioning: Comparison with Other Approaches. The monolayer and bilayer log$P$ values, as predicted by the present model (Table 3, the last line), are summarized in Table 1. The used approach takes into account the volume of individual strata, so the monolayer and bilayer data are described by the same model. Overall accumulation in both systems is predicted satisfactorily: the fit has the $r^2 = 0.941$ and the SD = 0.324 for 158 data points. We also examined other approaches that are used for modeling of overall accumulation in biological systems: the partition coefficients for the 1-octanol/water system using the logarithmized Collander equation (eq 1)[34] and the solvatochromic approach.[136] The correlations of the monolayer and bilayer accumulation for 95 and 63 compounds, respectively (Table 1), needed to be performed separately because the approaches do not include the volumes of the strata.

The correlations of the log$P_{m/w}$ and log$P_{b/w}$ values with the log$P_{O/W}$ values are very good, as indicated by the statistical indices, summarized in the first two lines of Table 5. The simplest approach using the $P_{O/W}$ values works well for neutral compounds, in accord with previous results.[33,137] In the overall linear trend, more precise linear correlations for polar and nonpolar chemicals, as well as for congeneric series were distinguishable.[33,107] The $P_{O/W}$ values are very well suited for QSAR modeling involving overall accumulation, especially if the $P_{O/W}$ parameter is a part of a more complex disposition function.[138] The situation may change for compounds with $P_{O/W} < 0.01$ (not present in our data set), which may be affected by the high water content (4% vol) in the water-saturated 1-octanol,[139] depending upon how much of this water can be used for hydration of drug molecules. The $P_{O/W}$ parameter did not perform well in correlations for liposome partitioning of ionizable compounds, forming mixtures of ionized and neutral molecules at physiological conditions because of different interactions of neutral and charged molecules.[140,141]

The solvatochromic approach was applied to the log$P_{m/w}$ and log$P_{b/w}$ data using the overall H-bond acidity, A; overall H-bond basicity, B; dipolarity/polarizability, S; excess molar refraction, E; and characteristic volume V, which were obtained using the Absolv software.[118] The estimated and experimental values of the solvatochromic properties $A-V$ are summarized in Table S2 in the Supporting Information. The log$P_{m/w}$ and log$P_{b/w}$ values are expressed as the linear combination of solvatochromic parameters, with the coefficients scaling individual parameters being denoted by the same letters, just using lowercase, as the parameters. The results, summarized in the last two lines of Table 5 demonstrate very good correlations, in accordance with a previous report.[137] Standard deviation of the regression coefficient a for the monolayer (Table 5, line 3) is larger than the coefficient itself. Removal of

a would provide similar statistical indices, but it was not performed to allow a comparison with other data sets. The solvatochromic approach is well suited for a direct modeling of overall accumulation in the DMPC liposomes. The higher number of optimized parameters makes its use in the disposition function[138] for QSAR models of biological effects more cumbersome.

The PPM approach was mainly developed for prediction of bilayer interactions with proteins and peptides but was also applied to partitioning of small organic molecules in the bilayer.[79] For 23 neutral and charged compounds, the model explained 65% of variance in the experimental binding free energies. The compounds were collected from several studies,[98,107,142−144] based on the criteria of conformational rigidity and composition limited to the C, H, N, O, and S atoms, for which the parameters were available. The performance may improve with more focus on partitioning of small molecules, distinguishing the interactions, which dominate in the bilayer partitioning of neutral and charged molecules, and expanding the set of parametrized atoms.

The COSMOmic approach[74] was used to predict the log$P_{b/w}$ values for more than 200 neutral compounds from two published sets.[145,146] The model explains 60% and 80% of experimental variance, respectively, and provides leave-one-out cross-validation results at similar levels. The use of MD simulations to obtain representative lipid geometries improved the performance to 81% to 92% of explained variance for the sets of 42−66 neutral compounds.[76,77]

Atomistic depth-constrained MD simulations with several force fields were compared for their ability to predict partition coefficients of 11 compounds.[96] The explained variance varies from 72% to 93% for individual force fields.

Applications of the Intrabilayer Distribution Model. The comparisons with other approaches show that our model predicts both the overall partition coefficient and the intrabilayer distribution. Other approaches focus mostly on the former aspect, and if they handle the distribution, they do not predict it well. The intrabilayer distribution is an important phenomenon, which plays key roles in drug action. It strongly affects at least two phenomena playing significant roles in drug development: interaction of compounds with the membrane proteins, which have binding sites only accessible from inside the bilayer and the trans-bilayer transport.

The connection intrabilayer distribution and membrane interactions are straightforward: only the fraction of the compound present at a proper bilayer depth is able to readily interact with the intrabilayer binding site. We expect that quantitative predictions of intrabilayer distribution will have a profound impact on modeling of drug interactions with the membrane proteins having the binding sites accessible from the bilayer, such as P-glycoprotein,[147] cytochromes P450,[148] cyclooxygenases,[149] and other targets.

The connection with the transport rates is less obvious, albeit logical. We hypothesized that a high transport rate requires a comparatively even intrabilayer distribution, in addition to sufficient overall bilayer accumulation. Too strong or too weak interactions with either H- or C-stratum or the H/C-interface create the bottlenecks, which slow down the transport.[3,33,150] Similar considerations for headgroups and core were used to justify the parabolic dependence of transport rates on the reference partition coefficients.[151] The hypothesis is also supported by the description of the steady-state permeability coefficient: its inverse value is equal to the sum of resistances in individual strata.[152,153] Each resistance is expressed as the ratio of the thickness and the product of the partition coefficient and the diffusion coefficient, all for the given stratum. As the drug–stratum interactions strengthen, the partition and diffusion coefficients increase and decrease, respectively. Consequently, optimum interaction strength could be expected as a condition for fast trans-bilayer diffusion. A slow-down may arise from a combination of a high partition coefficient and low diffusion coefficient or vice versa. Although preliminary data support our hypothesis,[3] a rigorous validation remains to be performed.

Trans-bilayer diffusion is a key factor for the rates of drug absorption and distribution in the body. While the importance of the absorption rate for oral bioavailability is well recognized, the role of distribution rate is unduly underappreciated. Most drugs are developed for oral administration, which often goes hand-in-hand with fast, whole-body distribution. However, for drugs with significant side effects, a toxicity reduction could be achieved by distribution that is restricted to the target body region, e.g., tumors for anticancer drugs. A limited distribution can be achieved by drugs with both targeted administration and slow trans-bilayer transport. While targeted administration is an intensively studied issue, the need for limited distribution is not generally recognized.

CONCLUSIONS

The calibrated model, logarithmized eq 10 combined with eq 11, with the optimized coefficient values given in the last line of Table 3, provides a prediction of both overall partitioning and drug distribution in individual strata of the DMPC bilayer for the compounds, for which the input data, the C16/W and the C16/DAcPC partition coefficients, and fragment solvation characteristics (Table 2) are available. The model was created for neutral compounds or compounds having negligible ionization under physiological conditions. The interfacial poses are generated using the algorithm described in Figure 2 and the accompanying text. The fragment-based partition coefficients of individual interfacial poses, P_{ij}, are calculated (eq 11) using the fragment solvation characteristics f in the DAcPC/W and C16/W systems for the fragments embedded in the headgroups and the core, respectively. The interfacial poses exhibit the Boltzmann distribution, with the fraction of the jth orientation being equal to $P_{ij}/\Sigma P_{ij}$.

The presented model is robust and stable, and has good predictive ability. The use of the established ClogP fragmentation scheme[35] allows the extension of these predictions for compounds, for which the ClogP fragment solvation parameters in the C16/DAcPC[55] and C16/W[97] are available. To the best of our knowledge, this is currently the only approach that allows reliable predictions of both overall partitioning and intrabilayer distribution for new compounds with available input data.

Overall, accumulation alone was also described well by other approaches: the O/W partition coefficients, the solvatochromic approach, COSMOmic combined with MD simulations, and atomistic MD simulations with some specialized force fields.

OUTLOOK

For the studied set of neutral molecules, the calibrated model showed good descriptivity, predictivity, and stability. In the future, if needed, the model can be expanded by including, e.g., electrostatics, molecular cross-section determining the disturbance of the most dense interface region, and entropy changes. The last aspect may be of lower significance thanks to the enthalpy–entropy compensation, which is a common phenomenon in partitioning.[42−44] Inclusion of electrostatic interactions, which may significantly contribute to bilayer partitioning of charged molecules,[43,143,154] is probably necessary because most drug molecules ionize under physiologic conditions.[155]

The model has been calibrated for the DMPC bilayer and needs to be expanded to other bilayer compositions. Extension to the bilayers consisting of PC with other saturated fatty acids should be accomplished by the use of adequate volume fractions for the headgroups and the core (eq 10). We assume that for bilayers composed of PC containing unsaturated fatty acids, the model could be directly recalibrated, with the main change expected in the Collander α and β coefficients for the core. This expectation is based on good Collander-type correlations for the partition coefficients of compounds measured in saturated and unsaturated hydrocarbons[156] and similar coefficients of the solvatochromic equation for the two-phase systems of n-hexadecane,[55] hexadec-1-ene,[157] and deca-1,9-diene[157,158] with water. The situation may be more complex, though, as indicated by experimental data for α-tocopherol showing the preferred location varying with PC fatty acid chains.[17] The effects of admixtures of other phospholipids and cholesterol to PC as the main phospholipid in mammalian membranes on bilayer distribution of compounds will require more complex model modifications.

ASSOCIATED CONTENT

ⓈSupporting Information

Table S1 contains, for all studied compounds, the interfacial poses and their predicted prevalences. Table S2 lists the solvatochromic parameters of the studied compounds and the aqueous pK_a values, where applicable. This material is available free of charge via the Internet at http://pubs.acs.org.

AUTHOR INFORMATION

Corresponding Author

*(S.B.) Department of Pharmaceutical Sciences, Albany College of Pharmacy and Health Sciences, Vermont Campus, 261 Mountain View Road, Colchester, Vermont 05446, United States. Phone: (802) 735-2615. Fax: (802) 654-0716. E-mail: stefan.balaz@acphs.edu.

Present Address

∥(V.L.) Simulations-Plus, Inc., Lancaster, California 93534, United States.

Notes

The authors declare no competing financial interest.

■ REFERENCES

(1) White, S. H. Translocons, thermodynamics, and the folding of membrane proteins. *FEBS Lett.* **2003**, *555*, 116–121.

(2) Goforth, R. L.; Chi, A. K.; Greathouse, D. V.; Providence, L. L.; Koeppe, R. E., II; Andersen, O. S. Hydrophobic coupling of lipid bilayer energetics to channel function. *J. Gen. Physiol.* **2003**, *121*, 477–493.

(3) Balaz, S. Lipophilicity in trans-bilayer transport and subcellular pharmacokinetics. *Perspect. Drug Discovery Des.* **2000**, *19*, 157–177.

(4) Wiener, M. C.; White, S. H. Structure of a fluid dioleoylphosphatidylcholine bilayer determined by joint refinement of x-ray and neutron diffraction data. III. Complete structure. *Biophys. J.* **1992**, *61*, 434–447.

(5) White, S. H.; King, G. I.; Cain, J. E. Location of hexane in lipid bilayers determined by neutron diffraction. *Nature* **1981**, *290*, 161–163.

(6) McIntosh, T. J. X-ray diffraction to determine the thickness of raft and nonraft bilayers. *Methods Mol. Biol.* **2007**, *398*, 221–230.

(7) Marrink, S. J.; Berendsen, H. J. C. Simulation of water transport through a lipid membrane. *J. Phys. Chem.* **1994**, *98*, 4155–4168.

(8) Alinchenko, M. G.; Anikeenko, A. V.; Medvedev, N. N.; Voloshin, V. P.; Mezei, M.; Jedlovszky, P. Morphology of voids in molecular systems. A Voronoi-Delaunay analysis of a simulated DMPC membrane. *J. Phys. Chem. B* **2004**, *108*, 19056–19067.

(9) Rabinovich, A. L.; Balabaev, N. K.; Alinchenko, M. G.; Voloshin, V. P.; Medvedev, N. N.; Jedlovszky, P. Computer simulation study of intermolecular voids in unsaturated phosphatidylcholine lipid bilayers. *J. Chem. Phys.* **2005**, *122*, 084906–1–084906/12.

(10) Edidin, M. The state of lipid rafts: From model membranes to cells. *Annu. Rev. Biophys. Biomol. Struct.* **2003**, *32*, 257–283.

(11) Hinderliter, A.; Biltonen, R. L.; Almeida, P. F. F. Lipid modulation of protein-induced membrane domains as a mechanism for controlling signal transduction. *Biochemistry* **2004**, *43*, 7102–7110.

(12) Pata, V.; Dan, N. Effect of membrane characteristics on phase separation and domain formation in cholesterol-lipid mixtures. *Biophys. J.* **2005**, *88*, 916–924.

(13) Tsamaloukas, A.; Szadkowska, H.; Heerklotz, H. Nonideal mixing in multicomponent lipid/detergent systems. *J. Phys.: Condens. Matter* **2006**, *18*, S1125–S1138.

(14) Bruce, A. Skeletal muscle lipids. II. Changes in phospholipid composition in man from fetal to middle age. *J. Lipid Res.* **1974**, *15*, 103–108.

(15) *Geigy Scientific Tables*, 8th ed.; Ciba-Geigy Corporation: West Caldwell, NJ, 1986; pp 221–223.

(16) Bruce, A. Skeletal muscle lipids. III. Changes in fatty acid composition of individual phosphoglycerides in man from fetal to middle age. *J. Lipid Res.* **1974**, *15*, 109–113.

(17) Marquardt, D.; Williams, J. A.; Kinnun, J. J.; Kucerka, N.; Atkinson, J.; Wassall, S. R.; Katsaras, J.; Harroun, T. A. Dimyristoyl phosphatidylcholine: A remarkable exception to α-tocopherol's membrane presence. *J. Am. Chem. Soc.* **2013**, *136*, 203–210.

(18) Potamitis, C.; Chatzigeorgiou, P.; Siapi, E.; Viras, K.; Mavromoustakos, T.; Hodzic, A.; Pabst, G.; Cacho-Nerin, F.; Laggner, P.; Rappolt, M. Interactions of the AT1 antagonist valsartan with dipalmitoyl-phosphatidylcholine bilayers. *Biochim. Biophys. Acta, Biomembr.* **2011**, *1808*, 1753–1763.

(19) Fotakis, C.; Megariotis, G.; Christodouleas, D.; Kritsi, E.; Zoumpoulakis, P.; Ntountaniotis, D.; Zervou, M.; Potamitis, C.; Hodzic, A.; Pabst, G.; Rappolt, M.; Mali, G.; Baldus, J.; Glaubitz, C.; Papadopoulos, M. G.; Afantitis, A.; Melagraki, G.; Mavromoustakos, T. Comparative study of the AT1 receptor prodrug antagonist candesartan cilexetil with other sartans on the interactions with membrane bilayers. *Biochim. Biophys. Acta, Biomembr.* **2012**, *1818*, 3107–3120.

(20) Moring, J.; Niego, L. A.; Ganley, L. M.; Trumbore, M. W.; Herbette, L. G. Interaction of the NMDA receptor noncompetetive antagonist MK 801 with model and native membranes. *Biophys. J.* **1994**, *67*, 2376–2386.

(21) Golden, G. A.; Rubin, R. T.; Mason, R. P. Steroid hormones partition to distinct sites in a model membrane bilayer: Direct demonstration by small-angle X-Ray diffraction. *Biochim. Biophys. Acta, Biomembr.* **1998**, *1368*, 161–166.

(22) Pebay, P. E.; Dufourc, E. J.; Szabo, A. G. Location of diphenyl-hexatriene and trimethylammonium-diphenyl-hexatriene in dipalmi-toylphosphatidylcholine bilayers by neutron diffraction. *Biophys. Chem.* **1994**, *53*, 45–56.

(23) Klacsova, M.; Bulacu, M.; Kucerka, N.; Uhrikova, D.; Teixeira, J.; Marrink, S. J.; Balgavy, P. The effect of aliphatic alcohols on fluid bilayers in unilamellar DOPC vesicles: A small-angle neutron scattering and molecular dynamics study. *Biochim. Biophys. Acta, Biomembr.* **2011**, *1808*, 2136–2146.

(24) Marquardt, D.; Williams, J. A.; Kucerka, N.; Atkinson, J.; Wassall, S. R.; Katsaras, J.; Harroun, T. A. Tocopherol activity correlates with its location in a membrane: A new perspective on the antioxidant vitamin E. *J. Am. Chem. Soc.* **2013**, *135*, 7523–7533.

(25) Henderson, J. M.; Iannucci, R. M.; Petersheim, M. An NMR study of pyridine associated with DMPC liposomes and magnetically ordered DMPC-surfactant mixed micelles. *Biophys. J.* **1994**, *67*, 238–249.

(26) Okamura, E.; Nakahara, M. NMR study directly determining drug delivery sites in phospholipid bilayer membranes. *J. Phys. Chem. B* **1999**, *103*, 3505–3509.

(27) Afri, M.; Ehrenberg, B.; Talmon, Y.; Schmidt, J.; Cohen, Y.; Frimer, A. A. Active oxygen chemistry within the liposomal bilayer Part III: Locating vitamin E, ubiquinol and ubiquinone and their derivatives in the lipid bilayer. *Chem. Phys. Lipids* **2004**, *131*, 107–121.

(28) Abdul-Wahid, M. S.; Neale, C.; Pomes, R.; Prosser, R. S. A solution NMR approach to the measurement of amphiphile immersion depth and orientation in membrane model systems. *J. Am. Chem. Soc.* **2009**, *131*, 6452–6459.

(29) Bartucci, R.; Mollica, P.; Sapia, P.; Sportelli, L. Procain interaction with DPPC multilayers. An ESR spin label investigation. *Appl. Magn. Reson.* **1998**, *15*, 181–195.

(30) Cimitan, S.; Lindgren, M. T.; Bertucci, C.; Danielson, U. H. Early absorption and distribution analysis of antitumor and anti-AIDS drugs: Lipid membrane and plasma protein interactions. *J. Med. Chem.* **2005**, *48*, 3536–3546.

(31) Afri, M.; Naqqash, M. E.; Frimer, A. A. Using fluorescence to locate intercalants within the lipid bilayer of liposomes, bioliposomes and erythrocyte ghosts. *Chem. Phys. Lipids* **2011**, *164*, 759–765.

(32) Asuncion-Punzalan, E.; London, E. Control of the depth of molecules within membranes by polar groups: Determination of the location of anthracene-labeled probes in model membranes by parallax analysis of nitroxide-labeled phospholipid induced fluorescence quenching. *Biochemistry* **1995**, *34*, 11460–11466.

(33) Balaz, S. Modeling kinetics of subcellular disposition of chemicals. *Chem. Rev.* **2009**, *109*, 1793–1899.

(34) Collander, R. The partition of organic compounds between higher alcohols and water. *Acta Chem. Scand.* **1951**, *5*, 774–780.

(35) Hansch, C.; Leo, A. *Substituent Constants for Correlation Analysis in Chemistry and Biology*; Wiley: New York, 1979; pp 1–339.

(36) Giesen, D. J.; Hawkins, G. D.; Liotard, D. A.; Cramer, C. J.; Truhlar, D. G. A universal model for the quantum mechanical calculation of free energies of solvation in non-aqueous solvents. *Theor. Chem. Acc.* **1997**, *98*, 85–109.

(37) White, S. H.; Ladokhin, A. S.; Jayasinghe, S.; Hristova, K. How membranes shape protein structure. *J. Biol. Chem.* **2001**, *276*, 32395–32398.

(38) Hansch, C.; Leo, A. *Exploring QSAR: Fundamentals and Applications in Chemistry and Biology*; American Chemical Society: Washington, DC, 1995.

(39) Kamlet, M. J.; Abboud, J. L. M.; Taft, R. W. An examination of linear solvation energy relationships. *Prog. Phys. Org. Chem.* **1981**, *13*, 485−630.

(40) Hammett, L. P. Linear free-energy relation in rate and equilibrium phenomena. *Trans. Faraday Soc.* **1938**, *34*, 156−165.

(41) Abraham, M. H.; Le, J. The correlation and prediction of the solubility of compounds in water using an amended solvation energy relationship. *J. Pharm. Sci.* **1999**, *88*, 868−880.

(42) Katz, Y.; Diamond, J. M. Thermodynamic constants for nonelectrolyte partition between dimyristoyl lecithin and water. *J. Membr. Biol.* **1974**, *17*, 101−120.

(43) Smith, R. A.; Porter, E. G.; Miller, K. W. The solubility of anesthetic gases in lipid bilayers. *Bichim. Biophys. Acta* **1981**, *645*, 327−338.

(44) Xiang, T. X.; Anderson, B. D. Molecular dissolution processes in lipid bilayers: A molecular dynamics simulation. *J. Chem. Phys.* **1999**, *110*, 1807−1818.

(45) Katz, Y.; Diamond, J. M. Nonsolvent water in liposomes. *J. Membr. Biol.* **1974**, *17*, 87−100.

(46) Nagle, J. F.; Zhang, R.; Tristram-Nagle, S.; Sun, W.; Petrache, H. I.; Suter, R. M. X-ray structure determination of fully hydrated Lα phase dipalmitoylphosphatidylcholine bilayers. *Biophys. J.* **1996**, *70*, 1419−1431.

(47) Balgavy, P.; Dubnickova, M.; Kucerka, N.; Kiselev, M. A.; Yaradaikin, S. P.; Uhrikova, D. Bilayer thickness and lipid interface area in unilamellar extruded 1,2-diacylphosphatidylcholine liposomes: A small-angle neutron scattering study. *Biochim. Biophys. Acta* **2001**, *1512*, 40−52.

(48) Kucerka, N.; Kiselev, M. A.; Balgavy, P. Determination of bilayer thickness and lipid surface area in unilamellar dimyristoylphosphatidylcholine vesicles from small-angle neutron scattering curves: A comparison of evaluation methods. *Eur. Biophys. J.* **2004**, *33*, 328−334.

(49) Wiener, M. C.; White, S. H. Structure of a fluid dioleoylphosphatidylcholine bilayer determined by joint refinement of x-ray and neutron diffraction data. II. Distribution and packing of terminal methyl groups. *Biophys. J.* **1992**, *61*, 428−433.

(50) Venable, R. M.; Zhang, Y.; Hardy, B. J.; Pastor, R. W. Molecular dynamics simulations of a lipid bilayer and of hexadecane: An investigation of membrane fluidity. *Science* **1993**, *262*, 223−226.

(51) Xiang, T. X.; Chen, X.; Anderson, B. D. Transport methods for probing the barrier domain of lipid bilayer membranes. *Biophys. J.* **1992**, *63*, 78−88.

(52) Xiang, T.; Xu, Y.; Anderson, B. D. The barrier domain for solute permeation varies with lipid bilayer phase structure. *J. Membr. Biol.* **1998**, *165*, 77−90.

(53) Xiang, T. X.; Anderson, B. D. The relationship between permeant size and permeability in lipid bilayer membranes. *J. Membr. Biol.* **1994**, *140*, 111−122.

(54) Lukacova, V.; Peng, M.; Tandlich, R.; Hinderliter, A.; Balaz, S. Partitioning of organic compounds in phases imitating the headgroup and core regions of phospholipid bilayers. *Langmuir* **2006**, *22*, 1869−1874.

(55) Lukacova, V.; Natesan, S.; Peng, M.; Tandlich, R.; Wang, Z.; Lynch, S.; Subramaniam, R.; Balaz, S. Structural determinants of drug partitioning in surrogates of phosphatidylcholine bilayer strata. *Mol. Pharmaceutics* **2013**, *10*, 3684−3696.

(56) Ahmed, M.; Burton, J. S.; Hadgraft, J.; Kellaway, I. W. Thermodynamics of partitioning and efflux of phenothiazines from liposomes. *J. Membr. Biol.* **1981**, *58*, 181−189.

(57) Dulfer, W. J.; Govers, H. A. J. Membrane water partitioning of polychlorinated biphenyls in small unilamellar vesicles of four saturated phosphatidylcholines. *Environ. Sci. Technol.* **1995**, *29*, 2548−2554.

(58) De Young, L. R.; Dill, K. A. Partitioning of nonpolar solutes into bilayers and amorphous *n*-alkanes. *J. Phys. Chem.* **1990**, *94*, 801−809.

(59) Seydel, J. K.; Wiese, M. *Drug-Membrane Interactions: Analysis, Drug Distribution, Modeling*; Wiley-VCH: Weinheim, Germany, 2003; pp 1−349.

(60) Ayton, G. S.; Noid, W. G.; Voth, G. A. Multiscale modeling of biomolecular systems: In serial and in parallel. *Curr. Opin. Struct. Biol.* **2007**, *17*, 192−198.

(61) Pandit, S. A.; Scott, H. L. Simulations and models of lipid bilayers. *Soft Matter* **2008**, *4*, 1−82.

(62) Brasseur, R.; Dellers, M.; Malaisse, W. J.; Ruysschaert, J. M. Conformational analysis of the calcium-A23187 complex at a lipid-water interface. *Proc. Natl. Acad. Sci. U.S.A.* **1982**, *79*, 2895−2897.

(63) Brasseur, R.; Laurent, G.; Ruysschaert, J. M.; Tulkens, P. Interactions of aminoglycoside antibiotics with negatively charged lipid layers. Biochemical and conformational studies. *Biochem. Pharmacol.* **1984**, *33*, 629−637.

(64) Edholm, O.; Jaehnig, F. The structure of a membrane-spanning polypeptide studied by molecular dynamics. *Biophys. Chem.* **1988**, *30*, 279−292.

(65) Ram, P.; Kim, E.; Thomson, D. S.; Howard, K. P.; Prestegard, J. H. Computer modelling of glycolipids at membrane surfaces. *Biophys. J.* **1992**, *63*, 1530−1535.

(66) Sanders, C. R.; Schwonek, J. P. An approximate model and empirical energy function for solute interactions with a water-phosphatidylcholine interface. *Biophys. J.* **1993**, *65*, 1207−1218.

(67) Ducarme, P.; Rahman, M.; Brasseur, R. IMPALA: A simple restraint field to simulate the biological membrane in molecular structure studies. *Proteins* **1998**, *30*, 357−371.

(68) Honig, B.; Nicholls, A. Classical electrostatics in biology and chemistry. *Science* **1995**, *268*, 1144−1149.

(69) Cramer, C. J.; Truhlar, D. G. A universal approach to solvation modeling. *Acc. Chem. Res.* **2008**, *41*, 760−768.

(70) Oren, I.; Fleishman, S. J.; Kessel, A.; Ben Tal, N. Free diffusion of steroid hormones across biomembranes: A simplex search with implicit solvent model calculations. *Biophys. J.* **2004**, *87*, 768−779.

(71) Sitkoff, D.; Ben Tal, N.; Honig, B. Calculation of alkane to water solvation free energies using continuum solvent models. *J. Phys. Chem.* **1996**, *100*, 2744−2752.

(72) Tanizaki, S.; Feig, M. Molecular dynamics simulations of large integral membrane proteins with an implicit membrane model. *J. Phys. Chem. B* **2006**, *110*, 548−556.

(73) Feig, M. Implicit membrane models for membrane protein simulation. *Methods Mol. Biol.* **2008**, *443*, 181−196.

(74) Klamt, A.; Huniar, U.; Spycher, S.; Keldenich, J. COSMOmic: A mechanistic approach to the calculation of membrane-water partition coefficients and internal distributions within membranes and micelles. *J. Phys. Chem. B* **2008**, *112*, 12148−12157.

(75) Klamt, A. *COSMO-RS: From Quantum Chemistry to Fluid Phase Thermodynamics and Drug Design*; Elsevier: New York, 2005; pp 1−200.

(76) Jakobtorweihen, S.; Ingram, T.; Smirnova, I. Combination of COSMOmic and molecular dynamics simulations for the calculation of membrane-water partition coefficients. *J. Comput. Chem.* **2013**, *34*, 1332−1340.

(77) Ingram, T.; Storm, S.; Kloss, L.; Mehling, T.; Jakobtorweihen, S.; Smirnova, I. Prediction of micelle/water and liposome/water partition coefficients based on molecular dynamics simulations, COSMO-RS, and COSMOmic. *Langmuir* **2013**, *29*, 3527−3537.

(78) Lomize, A. L.; Pogozheva, I. D.; Mosberg, H. I. Anisotropic solvent model of the lipid bilayer. 1. Parameterization of long-range electrostatics and first solvation shell effects. *J. Chem. Inf. Model.* **2011**, *51*, 918−929.

(79) Lomize, A. L.; Pogozheva, I. D.; Mosberg, H. I. Anisotropic solvent model of the lipid bilayer. 2. Energetics of insertion of small molecules, peptides, and proteins in membranes. *J. Chem. Inf. Model.* **2011**, *51*, 930−946.

(80) Shelley, J. C.; Shelley, M. Y.; Reeder, R. C.; Bandyopadhyay, S.; Moore, P. B.; Klein, M. L. Simulations of phospholipids using a coarse grain model. *J. Phys. Chem. B* **2001**, *105*, 9785−9792.

(81) Wassenaar, T. A.; Ingolfsson, H. I.; Priess, M.; Marrink, S. J.; Schaefer, L. V. Mixing MARTINI: Electrostatic coupling in hybrid atomistic-coarse-grained biomolecular simulations. *J. Phys. Chem. B* **2013**, *117*, 3516−3530.

(82) Zavadlav, J.; Melo, M. N.; Cunha, A. V.; De Vries, A. H.; Marrink, S. J.; Praprotnik, M. Adaptive resolution simulation of MARTINI solvents. *J. Chem. Theory Comput.* **2014**, *10*, 2591–2598.

(83) Wassenaar, T. A.; Pluhackova, K.; Bockmann, R. A.; Marrink, S. J.; Tieleman, D. P. Going backward: A flexible geometric approach to reverse transformation from coarse grained to atomistic models. *J. Chem. Theory Comput.* **2014**, *10*, 676–690.

(84) Bassolino-Klimas, D.; Alper, H. E.; Stouch, T. R. Solute diffusion in lipid bilayer membranes: An atomic level study by molecular dynamics simulation. *Biochemistry* **1993**, *32*, 12624–12637.

(85) Bassolino-Klimas, D.; Alper, H. E.; Stouch, T. R. Mechanism of solute diffusion through lipid bilayer membranes by molecular dynamics simulation. *J. Am. Chem. Soc.* **1995**, *117*, 4118–4129.

(86) Alper, H. E.; Stouch, T. R. Orientation and diffusion of a drug analog in biomembranes: Molecular dynamics simulations. *J. Phys. Chem.* **1995**, *99*, 5724–5731.

(87) Huang, P.; Bertaccini, E.; Loew, G. H. Molecular dynamics simulation of anesthetic-phospholipid bilayer interactions. *J. Biomol. Struct. Dyn.* **1995**, *12*, 725–754.

(88) Huang, P.; Loew, G. H. Interaction of an amphiphilic peptide with a phospholipid bilayer surface by molecular dynamics simulation study. *J. Biomol. Struct. Dyn.* **1995**, *12*, 937–956.

(89) Bemporad, D.; Luttmann, C.; Essex, J. W. Behaviour of small solutes and large drugs in a lipid bilayer from computer simulations. *Biochim. Biophys. Acta, Biomembr.* **2005**, *1718*, 1–21.

(90) Tejwani, R. W.; Davis, M. E.; Anderson, B. D.; Stouch, T. R. An atomic and molecular view of the depth dependence of the free energies of solute transfer from water into lipid bilayers. *Mol. Pharmaceutics* **2011**, *8*, 2204–2215.

(91) Tejwani, R. W.; Davis, M. E.; Anderson, B. D.; Stouch, T. R. Functional group dependence of solute partitioning to various locations within a DOPC bilayer: A comparison of molecular dynamics simulations with experiment. *J. Pharm. Sci.* **2011**, *100*, 2136–2146.

(92) Park, S.; Khalili-Araghi, F.; Tajkhorshid, E.; Schulten, K. Free energy calculation from steered molecular dynamics simulations using Jarzynski's equality. *J. Chem. Phys.* **2003**, *119*, 3559–3566.

(93) Pastor, R. W.; MacKerell, A. D. Development of the CHARMM force field for lipids. *J. Phys. Chem. Lett.* **2011**, *2*, 1526–1532.

(94) Jaembeck, J. P. M.; Lyubartsev, A. P. Derivation and systematic validation of a refined all-atom force field for phosphatidylcholine lipids. *J. Phys. Chem. B* **2012**, *116*, 3164–3179.

(95) Dickson, C. J.; Madej, B. D.; Skjevik, A. A.; Betz, R. M.; Teigen, K.; Gould, I. R.; Walker, R. C. Lipid14: The Amber lipid force field. *J. Chem. Theory Comput.* **2014**, *10*, 865–879.

(96) Paloncyova, M.; Fabre, G.; DeVane, R. H.; Trouillas, P.; Berka, K.; Otyepka, M. Benchmarking of force fields for molecule-membrane interactions. *J. Chem. Theory Comput.* **2014**, *10*, 4143–4151.

(97) Natesan, S.; Wang, Z.; Lukacova, V.; Peng, M.; Subramaniam, R.; Lynch, S.; Balaz, S. Structural determinants of drug partitioning in n-hexadecane/water system. *J. Chem. Inf. Model.* **2013**, *53*, 1424–1435.

(98) Lukacova, V.; Peng, M.; Fanucci, G.; Tandlich, R.; Hinderliter, A.; Maity, B.; Mannivanan, E.; Cook, G. R.; Balaz, S. Drug-membrane interactions studied in phospholipid monolayers adsorbed on nonporous alkylated microspheres. *J. Biomol. Screening* **2007**, *12*, 186–202.

(99) Macdonald, R. C.; MacDonald, R. I.; Menco, B. P.; Takeshita, K.; Subbarao, N. K.; Hu, L. R. Small-volume extrusion apparatus for preparation of large, unilamellar vesicles. *Biochim. Biophys. Acta* **1991**, *1061*, 297–303.

(100) Anderson, R. L.; Davis, S. An organic phosphorus assay which avoids the use of hazardous perchloric acid. *Clin. Chim. Acta* **1982**, *121*, 111–116.

(101) *Origin 7.0*; Origin Lab: Northampton, MA, 2002.

(102) Heerklotz, H.; Seelig, J. Titration calorimetry of surfactant-membrane partitioning and membrane solubilization. *Biochim. Biophys. Acta* **2000**, *1508*, 69–85.

(103) Trandum, C.; Westh, P.; Jorgensen, K.; Mouritsen, O. G. Use of isothermal titration calorimetry to study the interaction of short-chain alcohols with lipid membranes. *Thermochim. Acta* **1999**, *328*, 129–135.

(104) Zhang, F.; Rowe, E. S. Titration calorimetric and differential scanning calorimetric studies of the interactions of n-butanol with several phases of dipalmitoylphosphatidylcholine. *Biochemistry* **1992**, *31*, 2005–2011.

(105) Welti, R.; Mullikin, L. J.; Yoshimura, T.; Helmkamp, G. M., Jr. Partition of amphiphilic molecules into phospholipid vesicles and human erythrocyte ghosts: Measurements by ultraviolet difference spectroscopy. *Biochemistry* **1984**, *23*, 6086–6091.

(106) Avdeef, A.; Box, K. J.; Comer, J. E.; Hibbert, C.; Tam, K. Y. pH-metric logP 10. Determination of liposomal membrane-water partition coefficients of ionizable drugs. *Pharm. Res.* **1998**, *15*, 209–215.

(107) Vaes, W. H. J.; Ramos, E. U.; Hamwijk, C.; van Holsteijn, I.; Blaauboer, B. J.; Seinen, W.; Verhaar, H. J. M.; Hermens, J. L. M. Solid phase microextraction as a tool to determine membrane/water partition coefficients and bioavailable concentrations in in vitro systems. *Chem. Res. Toxicol.* **1997**, *10*, 1067–1072.

(108) Kamaya, H.; Kaneshima, S.; Ueda, I. Partition equilibrium of inhalation anesthetics and alcohols between water and membranes of phospholipids with varying chain-lengths. *Biochim. Biophys. Acta* **1981**, *646*, 135–142.

(109) Anderson, N. H.; Davis, S. S.; James, M.; Kojima, I. Thermodynamics of distribution of p-substituted phenols between aqueous solution and organic solvents and phospholipid vesicles. *J. Pharm. Sci.* **1983**, *72*, 443–448.

(110) Miyoshi, H.; Maeda, H.; Tokutake, N.; Fujita, T. Quantitative analysis of partition behavior of substituted phenols from aqueous phase into liposomes made of lecithin and various lipids. *Chem. Soc. Jpn.* **1987**, *60*, 4357–4362.

(111) Gobas, F. A. P. C.; Lahittete, J. M.; Garofalo, G.; Shiu, W. Y.; Mackay, D. A novel method for measuring membrane-water partition coefficients of hydrophobic organic chemicals: Comparison with 1-octanol-water partitioning. *J. Pharm. Sci.* **1988**, *77*, 265–272.

(112) Escher, B. I.; Schwarzenbach, R. P. Partitioning of substituted phenols in liposome-water, biomembrane-water, and octanol-water systems. *Environ. Sci. Technol.* **1996**, *30*, 260–270.

(113) Fruttero, R.; Caron, G.; Fornatto, E.; Boschi, D.; Ermondi, G.; Gasco, A.; Carrupt, P. A.; Testa, B. Mechanisms of liposomes/water partitioning of (p-methylbenzyl)alkylamines. *Pharm. Res.* **1998**, *15*, 1407–1413.

(114) Silvius, J. R. Thermotropic phase transitions of pure lipids in model membranes and their modifications by membrane proteins. In *Lipid-Protein Interactions*; Jost, P. C., Griffith, O. H., Eds.; Wiley and Sons: New York, 1982; pp 239–281.

(115) Rogers, J. A.; Davis, S. S. Functional group contributions to the partitioning of phenols between liposomes and water. *Biochim. Biophys. Acta* **1980**, *598*, 392–404.

(116) Redman-Furey, N. L.; Antinore, M. J. Determination of partition coefficients between dimyristoylphosphatidylcholine and water using differential scanning calorimetry. *Anal. Chim. Acta* **1991**, *251*, 79–81.

(117) Muller, M. T.; Zehnder, A. J. B.; Escher, B. I. Liposome-water and octanol-water partitioning of alcohol ethoxylates. *Environ. Toxicol. Chem.* **1999**, *18*, 2191–2198.

(118) *ACD/Percepta*, Build 2203; Advanced Chemistry Development, Inc.: Toronto, Canada, 2013.

(119) *Bio-Loom*; BioByte Corp.: Claremont, CA, 2006.

(120) Abraham, M. H.; Chadha, H. S.; Whiting, G. S.; Mitchell, R. C. Hydrogen bonding. 32. An analysis of water-octanol and water-alkane partitioning and the delta log P parameter of Seiler. *J. Pharm. Sci.* **1994**, *83*, 1085–1100.

(121) Bemporad, D.; Luttmann, C.; Essex, J. W. Computer simulation of small molecule permeation across a lipid bilayer: Dependence on bilayer properties and solute volume, size, and cross-sectional area. *Biophys. J.* **2004**, *87*, 1–13.

(122) *Solver*, Premium Platform v 10.5; Frontline Systems Inc.: Incline Village, NV, 2011.

(123) Hauser, H.; Pascher, I.; Pearson, R. H.; Sundell, S. Preferred conformation and molecular packing of phosphatidylethanolamine and phosphatidylcholine. *Biochim. Biophys. Acta* **1981**, *650*, 21−51.

(124) Eisenberg, D.; Weiss, R. M.; Terwilliger, T. C. The helical hydrophobic moment: A measure of the amphiphilicity of a helix. *Nature* **1982**, *299*, 371−374.

(125) Brasseur, R.; Vandenbosch, C.; Van den Bossche, H.; Ruysschaert, J. M. Mode of insersion of miconazole ketonazole and deacylated ketoconazole in lipid layers: A conformational analysis. *Biochem. Pharmacol.* **1983**, *32*, 2175−2180.

(126) Fischer, H.; Kansy, M.; Bur, D. CAFCA: A novel tool for the calculation of amphiphilic properties of charged drug molecules. *Chimia* **2000**, *54*, 640−645.

(127) Kessel, A.; Musafia, B.; Ben-Tal, N. Continuum solvent model studies of the interactions of an anticonvulsant drug with a lipid bilayer. *Biophys. J.* **2001**, *80*, 2536−2545.

(128) Kaiser, R. D.; London, E. Location of diphenylhexatriene (DPH) and its derivatives within membranes: Comparison of different fluorescence quenching analyses of membrane depth. *Biochemistry* **1998**, *37*, 8180−8190.

(129) Kachel, K.; Asuncion-Punzalan, E.; London, E. Anchoring of tryptophan and tyrosine analogs at the hydrocarbon-polar boundary in model membrane vesicles: Parallax analysis of fluorescence quenching induced by nitroxide-labeled phospholipids. *Biochemistry* **1995**, *34*, 15475−15479.

(130) Barry, J. A.; Gawrisch, K. Direct NMR Evidence for ethanol binding to the lipid-water interface of phospholipid bilayers. *Biochemistry* **1994**, *33*, 8082−8088.

(131) Ho, C.; Stubbs, C. D. Effect of n-alkanols on lipid bilayer hydration. *Biochemistry* **1997**, *36*, 10630−10637.

(132) Mitchell, D. C.; Lawrence, J. T. R.; Litman, B. J. Primary alcohols modulate the activation of the G protein-coupled receptor rhodopsin by a lipid-mediated mechanism. *J. Biol. Chem.* **1996**, *271*, 19033−19036.

(133) Collander, R. Lipoid solubility. *Acta Physiol. Scand.* **1947**, *13*, 363−381.

(134) Gaede, H. C.; Yau, W. M.; Gawrisch, K. Electrostatic contributions to indole-lipid interactions. *J. Phys. Chem. B* **2005**, *109*, 13014−13023.

(135) Minobe, M.; Sakurai, I.; Shibata, T.; Kawamura, Y. Effect of doping small aromatic molecules on the physical properties and liposomal structure of lecithin. *Mol. Cryst. Liq. Cryst. Sci. Technol., Sect. A* **1998**, *319*, 75−87.

(136) Abraham, M. H.; Buist, G. J.; Grellier, P. L.; McGill, R. A.; Doherty, R. M.; Kamlet, M. J.; Taft, R. W.; Maroldo, S. G. Solubility properties in polymers and biological media. II. A new method for the characterisation of the adsorption of gases and vapours on solids. *J. Chromatogr.* **1987**, *409*, 15−27.

(137) Endo, S.; Escher, B. I.; Goss, K. U. Capacities of membrane lipids to accumulate neutral organic chemicals. *Environ. Sci. Technol.* **2011**, *45*, 5912−5921.

(138) Natesan, S.; Wang, T.; Lukacova, V.; Bartus, V.; Khandelwal, A.; Subramaniam, R.; Balaz, S. Cellular quantitative structure-activity relationship (cell-QSAR): Conceptual dissection of receptor binding and intracellular disposition in antifilarial activities of *Selwood antimycins*. *J. Med. Chem.* **2012**, *55*, 3699−3712.

(139) Margolis, S. A.; Levenson, M. Certification by the Karl Fischer method of the water content in SRM 2890, water saturated 1-octanol, and the analysis of associated inter-laboratory bias in the measurement process. *Fresenius' J. Anal. Chem.* **2000**, *367*, 1−7.

(140) Herbette, L. G.; Chester, D. W.; Rhodes, D. G. Structural analysis of drug molecules in biological membranes. *Biophys. J.* **1986**, *49*, 91−94.

(141) Balon, K.; Riebesehl, B. U.; Müller, B. W. Drug liposome partitioning as a tool for the prediction of human passive intestinal absorption. *Pharm. Res.* **1999**, *16*, 882−888.

(142) Avdeef, A. *Absorption and Drug Development: Solubility, Permeability, and Charge State*; Wiley: Hoboken, NJ, 2003.

(143) Escher, B. I.; Schwarzenbach, R. P.; Westall, J. C. Evaluation of liposome-water partitioning of organic acids and bases. 2. Comparison of experimental determination methods. *Environ. Sci. Technol.* **2000**, *34*, 3962−3968.

(144) Wimley, W. C.; White, S. H. Membrane partitioning: Distinguishing bilayer effects from the hydrophobic effect. *Biochemistry* **1993**, *32*, 6307−6312.

(145) Spycher, S.; Smejtek, P.; Netzeva, T. I.; Escher, B. I. Toward a class-independent quantitative structure-activity relationship model for uncouplers of oxidative phosphorylation. *Chem. Res. Toxicol.* **2008**, *21*, 911−927.

(146) Loidl-Stahlhofen, A.; Hartmann, T.; Schottner, M.; Rohring, C.; Brodowsky, H.; Schmitt, J.; Keldenich, J. Multilamellar liposomes and solid-supported lipid membranes (TRANSIL): Screening of lipid-water partitioning toward a high-throughput scale. *Pharm. Res.* **2001**, *18*, 1782−1788.

(147) Seelig, A.; Gatlik-Landwojtowicz, E. Inhibitors of multidrug efflux transporters: Their membrane and protein interactions. *Mini-Rev. Med. Chem.* **2005**, *5*, 135−151.

(148) Cojocaru, V.; Balali-Mood, K.; Sansom, M. S. P.; Wade, R. C. Structure and dynamics of the membrane-bound cytochrome P450 2C9. *PLoS Comput. Biol.* **2011**, *7*, e1002152.

(149) Luong, C.; Miller, A.; Barnett, J.; Chow, J.; Ramesha, C.; Browner, M. F. Flexibility of the NSAID binding site in the structure of human cyclooxygenase-2. *Nat. Struct. Biol.* **1996**, *3*, 927−933.

(150) Balaz, S.; Wiese, M.; Seydel, J. K. A time hierarchy-based model for kinetics of drug disposition and its use in quantitative structure-activity relationships. *J. Pharm. Sci.* **1992**, *81*, 849−857.

(151) Hansch, C.; Fujita, T. ρ-σ-π analysis. A method for the correlation of biological activity and chemical structure. *J. Am. Chem. Soc.* **1964**, *86*, 1616−1626.

(152) Zwolinski, B. J.; Eyring, H.; Reese, C. E. Diffusion and membrane permeability. I. *J. Phys. Colloid Chem.* **1949**, *53*, 1426−1453.

(153) Scheuplein, R. J. The application of rate theory to complex multibarrier flow coordinates: Membrane permeability. *J. Theor. Biol.* **1968**, *18*, 72−91.

(154) Escher, B. I.; Schwarzenbach, R. P.; Westall, J. C. Evaluation of liposome-water partitioning of organic acids and bases. 1. Development of a sorption model. *Environ. Sci. Technol.* **2000**, *34*, 3954−3961.

(155) Wishart, D. S.; Knox, C.; Guo, A. C.; Cheng, D.; Shrivastava, S.; Tzur, D.; Gautam, B.; Hassanali, M. DrugBank: A knowledgebase for drugs, drug actions and drug targets. *Nucleic Acids Res.* **2008**, *36*, D901−D906.

(156) Xiang, T. X.; Anderson, B. D. Substituent contributions to the transport of substituted *p*-toluic acids across lipid bilayer membranes. *J. Pharm. Sci.* **1994**, *83*, 1511−1518.

(157) Abraham, M. H.; Acree, W. E. Linear free-energy relationships for water/hexadec-1-ene and water/deca-1,9-diene partitions, and for permeation through lipid bilayers: Comparison of permeation systems. *New J. Chem.* **2012**, *36*, 1798−1806.

(158) Nitsche, J. M.; Kasting, G. B. A correlation for 1,9-decadiene/water partition coefficients. *J. Pharm. Sci.* **2012**, *102*, 136−144.